

One-Pass Trajectory Simplification Using the Synchronous Euclidean Distance

Xuelian Lin · Jiahao Jiang · Shuai Ma · Yimeng Zuo · Chunming Hu

Received: xxx, 2017 / Accepted: xxx, 2018

Abstract Various mobile devices have been used to collect, store and transmit tremendous trajectory data, and it is known that raw trajectory data seriously wastes the storage, network band and computing resource. To attack this issue, one-pass line simplification (LS) algorithms have been developed, by compressing data points in a trajectory to a set of continuous line segments. However, these algorithms adopt the *perpendicular Euclidean distance*, and none of them uses the *synchronous Euclidean distance* (SED), and cannot support spatio-temporal queries. To do this, we develop two one-pass error bounded trajectory simplification algorithms (CISED-S and CISED-W) using SED, based on a novel spatio-temporal cone intersection technique. Using four real-life trajectory datasets, we experimentally show that our approaches run fast as well as have good compression ratios. In terms of running time, algorithms CISED-S and CISED-W are on average 3 times faster than SQUISH-E (the fastest existing LS algorithm using SED). In terms of compression ratios, CISED-S is close to and CISED-W is on average 19.6% better than DPSED (the existing sub-optimal LS algorithm using SED having the best compression ratios), and they are 21.1% and 42.4% better than SQUISH-E on average, respectively.

1 Introduction

Various mobile devices, such as smart-phones, on-board diagnostics, personal navigation devices, and wearable

smart devices, use their sensors to collect massive trajectory data of moving objects at a certain sampling rate (e.g., a data point every 5 seconds), which is transmitted to cloud servers for various applications such as location based services and trajectory mining. Transmitting and storing raw trajectory data consumes too much network bandwidth and storage capacity [2, 5, 15–17, 20, 22–24, 28, 35]. It is known that these issues can be resolved or greatly alleviated by trajectory compression techniques via removing redundant data points of trajectories [2, 4, 5, 7, 10, 12, 15–18, 20, 23, 24, 28], among which the piece-wise line simplification technique is widely used [2, 4, 5, 7, 15–17, 20, 23], due to its distinct advantages: (a) simple and easy to implement, (b) no need of extra knowledge and suitable for freely moving objects, and (c) bounded errors with good compression ratios [15, 28].

Originally, line simplification (LS) algorithms adopt the *perpendicular Euclidean distance* (PED) as a metric to compute the errors, e.g., $|\overrightarrow{P_4 P_4^*}|$ is the PED of data point P_4 to line segment $P_0 P_{10}$ in Figure 1 (left). Line simplification algorithms using PED have good compression ratios [2, 5, 7, 12, 15, 16, 23, 35]. However, when using PED, a spatio-temporal query, e.g., “the position of a moving object at time t ”, on the compressed trajectories will return an approximate point P' whose distance to the actual position P of the moving object at time t is unbounded.

The *synchronous Euclidean distance* (SED) was then introduced for trajectory compression to support the above spatio-temporal queries, where the approximate point P' was referred to as the approximate temporally *synchronized data point* [20]. Intuitively, given a sub-trajectory $[P_s, \dots, P_e]$ to be simplified, a synchronized data point P'_i ($s < i < e$) is a point on line seg-

X. Lin, J. Jiang, S. Ma (correspondence), Y. Zuo and C. Hu
Beijing Advanced Innovation Center for Big Data and Brain
Computing (BDBC), Beihang University, China.
E-mail: {linxl, jiangjh, mashuai, zuoyim, hucm}@buaa.edu.cn

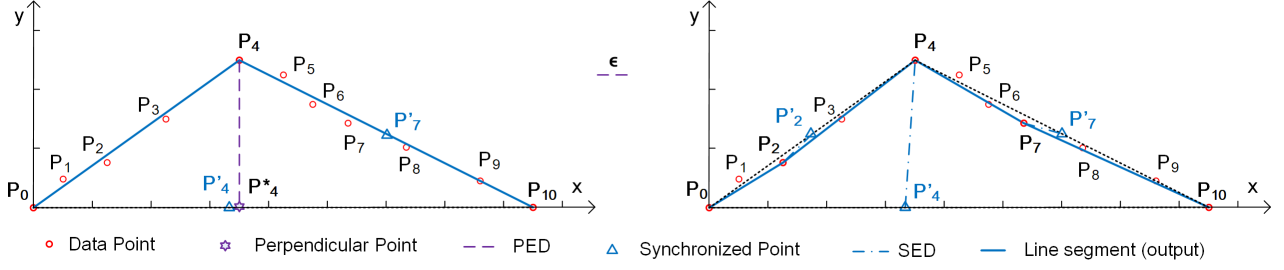


Fig. 1 A trajectory $\vec{T}[P_0, \dots, P_{10}]$ with eleven points is represented by two (left) and four (right) continuous line segments (solid blue), compressed by the Douglas-Peucker algorithm [7] using PED and SED, respectively. The Douglas-Peucker algorithm firstly creates line segment $\overrightarrow{P_0P_{10}}$, then it calculates the distance of each point in the trajectory to $\overrightarrow{P_0P_{10}}$. It finds that point P_4 has the maximum distance to $\overrightarrow{P_0P_{10}}$, and is greater than the user defined threshold ϵ . Then it goes to compress sub-trajectories $[P_0, \dots, P_4]$ and $[P_4, \dots, P_{10}]$, separately.

ment $\overrightarrow{P_sP_e}$ satisfying $|\overrightarrow{P_sP_e}| \leq \epsilon$ and $|\overrightarrow{P_sP_i}| = \frac{P_i.t - P_s.t}{P_e.t - P_s.t}$, and SED is the Euclidean distance of a data point P_i to its *synchronized data point* P'_i on the line segment $\overrightarrow{P_sP_e}$. For example, in Figure 1, P'_4 is a *synchronized data point* of point P_4 w.r.t. line segment $\overrightarrow{P_0P_{10}}$, satisfying $|\overrightarrow{P_0P'_4}| = \frac{P_4.t - P_0.t}{P_{10}.t - P_0.t}$. The SED of point P_4 to line segment $\overrightarrow{P_0P_{10}}$ is $|\overrightarrow{P_4P'_4}|$. Indeed, the SED of a point to a line segment is always not less than the PED of the point to the line segment, thus, LS algorithms using SED may lead to more line segments. However, the use of SED ensures that the Euclidean distance between a data point and its synchronized point w.r.t. the corresponding line segment is limited within a distance bound ϵ . Hence, the above spatio-temporal query over the trajectories compressed by SED enabled approaches returns the synchronized point P' of a data point P within the bound ϵ .

The problem of finding the minimal number of line segments to represent the original polygonal lines w.r.t. an error bound ϵ is known as the “min-#” problem [3, 14], and there exists an optimal LS algorithm using SED that runs in $O(n^3)$ [14] (originally designed for PED), where n is the number of the original points. Due to the high time complexity, sub-optimal LS algorithms using SED have been developed for trajectory compression, including batch algorithms (e.g., Douglas-Peucker based algorithm DPSED [20]) and online algorithms (e.g., SQUISH-E [23]). However, these methods still have high time and/or space complexities, which hinders their utilities in resource-constrained devices.

Observe that linear LS algorithms using PED [8, 15, 36, 40, 42] have been developed, and they are more efficient for resource-constrained devices. The key idea to achieve a linear time complexity is by local distance checking in constant time, the *sector intersection* mechanism used in [8, 36, 40, 42] and the *fitting function* approach used in our preview work [15]. Unfortunately,

these techniques are designed specifically for PED, and can hardly be applied for SED.

Indeed, it is even more challenging to design one-pass LS algorithms using SED than using PED. To our knowledge, no one-pass LS algorithms using SED have been developed in the community yet.

Contributions. To this end, we propose two fast one-pass error bounded LS algorithms using SED for compressing trajectories with good compression ratios.

(1) We first develop a novel local synchronous distance checking approach, i.e., spatio-temporal Cone Intersection using the Synchronous Euclidean Distance (CISED). We further approximate the intersection of spatio-temporal cones with the intersection of a special class of regular polygons, and develop a fast regular polygon intersection algorithm, such that each data point in a trajectory is checked in $O(1)$ time during the entire process of trajectory simplification.

(2) We next develop two one-pass trajectory simplification algorithms CISED-S and CISED-W, achieving $O(n)$ time complexity and $O(1)$ space complexity, based on our local synchronous distance checking technique. Algorithm CISED-S belongs to strong simplification that only has original points in its outputs, while algorithm CISED-W belongs to weak simplification that allows interpolated data points in its outputs.

(3) Using four real-life trajectory datasets (Truck, ServiceCar, GeoLife, PrivateCar), we finally conduct an extensive experimental study, by comparing our methods CISED-S and CISED-W with the optimal LS algorithm using SED, DPSED [20] (the existing sub-optimal LS algorithm using SED having the best compression ratios) and SQUISH-E [23] (the fastest existing LS algorithm using SED).

For running time, algorithms CISED-S and CISED-W are on average 15.0, 3.2 and 14345.0 times faster than DPSED, SQUISH-E and the optimal LS algorithm on the test datasets, respectively. For compression ratios, algorithm CISED-S is better than SQUISH-E and

close to DPSED. The output sizes of CISED-S are on average 74.4%, 110.4% and 137.9% of SQUISH-E, DPSED and the optimal LS algorithm on the test datasets, respectively. Moreover, algorithm CISED-W is on average 54.9% and 81.6% better than SQUISH-E and DPSED on the test datasets, respectively.

It is worth pointing out that trajectory data is collected by mobile devices from GPS sensors, and these devices have range errors, which leads to data quality issues of trajectory data [27, 44]. However, the problem is beyond the scope of this study, and we focus on lossy simplification of trajectory data only.


Organization. The remainder of the article is organized as follows. Section 2 introduces the basic concepts and techniques. Section 3 presents our local synchronous distance checking method. Section 4 presents our one-pass trajectory simplification algorithms. Section 5 reports the experimental results, followed by related work in Section 6 and conclusion in Section 7. All proofs are provided in the Appendix.

2 Preliminaries

In this section, we first introduce basic concepts for piece-wise line based trajectory compression. We then describe the optimal LS algorithm and the *sector intersection* mechanism, and show how this mechanism can be used to speed up the LS algorithms using PED and why it cannot work with SED. Finally, we illustrate a convex polygon intersection algorithm, which serves as one of the fundamental components of our local synchronous distance checking method. Notations used are summarized in Table 1.

2.1 Basic Notations

We first introduce basic notations.

Points (P). A data point is defined as a triple $P(x, y, t)$, which represents that a moving object is located at *longitude* x and *latitude* y at *time* t . Note that data points can be viewed as points in a **three-dimension Euclidean space**. 

Trajectories (\ddot{T}). A trajectory $\ddot{T}[P_0, \dots, P_n]$ is a sequence of data points in a monotonically increasing order of their associated time values (*i.e.*, $P_i.t < P_j.t$ for any $0 \leq i < j \leq n$). Intuitively, a trajectory is the path (or track) that a moving object follows through space as a function of time [21].

Directed line segments (\mathcal{L}). A directed line segment (or line segment for simplicity) \mathcal{L} is defined as $\overrightarrow{P_s P_e}$, which represents the closed line segment that connects

Table 1 Summary of notations

Notations	Semantics
P	a data point
\ddot{T}	a trajectory \ddot{T} is a sequence of data points
$\overline{\mathcal{T}}$	a piece-wise line representation of a trajectory \ddot{T}
\mathcal{L}	a directed line segment
$\overrightarrow{P_s P_e}$	a directed line segment with the start point P_s and the end point P_e
$ \mathcal{L} $	the length of \mathcal{L} in the x-y 2D space
$ped(P, \mathcal{L})$	the perpendicular Euclidean distance of point P to line segment \mathcal{L}
$sed(P, \mathcal{L})$	the synchronous Euclidean distance of point P to line segment \mathcal{L}
ϵ	the error bound
\mathcal{S}	a sector
$\vec{A} \times \vec{B}$	the cross product of (vectors) \vec{A} and \vec{B}
$\mathcal{H}(\mathcal{L})$	The open half-plane to the left of \mathcal{L}
\mathcal{R}	a convex polygon
\mathcal{R}^*	the intersection of convex polygons
m	the maximum number of edges of a polygon
E^j	a group of edges labeled with j
$g(e)$	the label of an edge e of polygons
\mathcal{O}	a synchronous circle
\mathcal{C}	a spatio-temporal cone
\mathcal{O}^c	a cone projection circle
\sqcap	intersection of geometries
G	the reachability graph of a trajectory

the start point P_s and the end point P_e . Note that here P_s or P_e may not be a point in a trajectory \ddot{T} .

For the projection of a directed line segment \mathcal{L} on a x - y 2D space, where x and y are the longitude and latitude, respectively, we also use $|\mathcal{L}|$ and $\mathcal{L}.\theta \in [0, 2\pi)$ to denote the length of \mathcal{L} in the x-y 2D space, and its angle with the x -axis of the coordinate system (x, y) . That is, the projection of a directed line segment $\mathcal{L} = \overrightarrow{P_s P_e}$ on a x - y 2D space is treated as a triple $(P_s, |\mathcal{L}|, \mathcal{L}.\theta)$.

Piecewise line representation ($\overline{\mathcal{T}}$). A piece-wise line representation $\overline{\mathcal{T}}[\mathcal{L}_0, \dots, \mathcal{L}_m]$ ($0 < m \leq n$) of a trajectory $\ddot{T}[P_0, \dots, P_n]$ is a sequence of continuous directed line segments $\mathcal{L}_i = \overrightarrow{P_{s_i} P_{e_i}}$ ($i \in [0, m]$) of \ddot{T} such that $\mathcal{L}_0.P_{s_0} = P_0$, $\mathcal{L}_m.P_{e_m} = P_n$ and $\mathcal{L}_i.P_{e_i} = \mathcal{L}_{i+1}.P_{s_{i+1}}$ for all $i \in [0, m-1]$. Note that each directed line segment in $\overline{\mathcal{T}}$ essentially represents a continuous sequence of data points in \ddot{T} .

Perpendicular Euclidean Distance (PED). Given a data point P and a directed line segment $\mathcal{L} = \overrightarrow{P_s P_e}$, the perpendicular Euclidean distance (or simply perpendicular

ular distance) $ped(P, \mathcal{L})$ of point P to line segment \mathcal{L} is $\min\{|\overrightarrow{PQ}|\}$ for any point Q on $\overrightarrow{P_s P_e}$.

Synchronized points [20]. Given a sub-trajectory $\ddot{T}_s[P_s, \dots, P_e]$, the synchronized point P' of a data point $P \in \ddot{T}_s$, w.r.t. line segment $\overrightarrow{P_s P_e}$ is defined as follows: (1) $P'.x = P_s.x + w \cdot (P_e.x - P_s.x)$, (2) $P'.y = P_s.y + w \cdot (P_e.y - P_s.y)$ and (3) $P'.t = P.t$, where $w = \frac{P.t - P_s.t}{P_e.t - P_s.t}$.

Intuitively, a synchronized data point P'_i of P_i ($s < i < e$) is a point on $\overrightarrow{P_s P_e}$ satisfying $|\overrightarrow{P_s P'_i}| > 0$ and $\frac{|\overrightarrow{P_s P'_i}|}{|\overrightarrow{P_s P_e}|} = \frac{P_i.t - P_s.t}{P_e.t - P_s.t}$, which means that the object is moving from P_s to P_e at an average speed $\frac{|\overrightarrow{P_s P_e}|}{P_e.t - P_s.t}$, and its position at time t_i is point P'_i on $\overrightarrow{P_s P_e}$ having a distance of $\frac{P_i.t - P_s.t}{P_e.t - P_s.t} \cdot |\overrightarrow{P_s P_e}|$ to point P_s [4, 20, 41].

Synchronous Euclidean Distance (SED) [20]. Given a data point P and a directed line segment $\mathcal{L} = \overrightarrow{P_s P_e}$, the synchronous Euclidean distance (or simply synchronous distance) $sed(P, \mathcal{L})$ of P to \mathcal{L} is $|\overrightarrow{PP'}|$ that is the Euclidean distance from P to its synchronized point P' w.r.t. \mathcal{L} .

The use of PED brings better compression ratios, but the temporal information of data points is not available [20], which makes PED not suitable for spatio-temporal queries. In contrast, SED takes both spatial and temporal information of data points into consideration [20]. Hence SED is more suitable for spatio-temporal queries.

We illustrate these notations with examples.

Example 1 Consider Figure 1 again, in which

- (1) $\ddot{T}[P_0, \dots, P_{10}]$ is a trajectory having 11 data points,
- (2) the set of two continuous line segments $\{\overrightarrow{P_0 P_4}, \overrightarrow{P_4 P_{10}}\}$ (Left) and the set of four continuous line segments $\{\overrightarrow{P_0 P_2}, \overrightarrow{P_2 P_4}, \overrightarrow{P_4 P_7}, \overrightarrow{P_7 P_{10}}\}$ (Right) are two piecewise line representations of trajectory \ddot{T} ,
- (3) $ped(P_4, \overrightarrow{P_0 P_{10}}) = |\overrightarrow{P_4 P_4^*}|$, where P_4^* is the perpendicular point of P_4 w.r.t. line segment $\overrightarrow{P_0 P_{10}}$,
- (4) P'_4 is the synchronized point of P_4 w.r.t. line segment $\overrightarrow{P_0 P_{10}}$, satisfying $\frac{|\overrightarrow{P_0 P'_4}|}{|\overrightarrow{P_0 P_{10}}|} = \frac{P_4.t - P_0.t}{P_{10}.t - P_0.t} = \frac{4-0}{10-0} = \frac{2}{5}$, and
- (5) $sed(P_4, \overrightarrow{P_0 P_{10}}) = |\overrightarrow{P_4 P'_4}|$, $sed(P_2, \overrightarrow{P_0 P_4}) = |\overrightarrow{P_2 P'_2}|$ and $sed(P_7, \overrightarrow{P_4 P_{10}}) = |\overrightarrow{P_7 P'_7}|$, where points P'_4 , P'_2 and P'_7 are the synchronized points of P_4 , P_2 and P_7 w.r.t. line segments $\overrightarrow{P_0 P_{10}}$, $\overrightarrow{P_0 P_4}$ and $\overrightarrow{P_4 P_{10}}$, respectively. \square

Error bounded algorithms. Given a trajectory \ddot{T} and its compression algorithm \mathcal{A} using SED (respectively PED) that produces another trajectory \ddot{T}' , we say that algorithm \mathcal{A} is error bounded by ϵ if for each point P in \ddot{T} , there exist points P_j and P_{j+1} in \ddot{T}' such that such that $P_j.t \leq P.t \leq P_{j+1}.t$ and $sed(P, \mathcal{L}(P_j, P_{j+1})) \leq \epsilon$ (respectively $ped(P, \mathcal{L}(P_j, P_{j+1})) \leq \epsilon$).

2.2 The Optimal LS Algorithm

Given a trajectory $\ddot{T}[P_0, \dots, P_n]$ and an error bound ϵ , the optimal trajectory simplification problem, as formulated by Imai and Iri in [14], can be solved in two steps: (1) construct a reachability graph G of \ddot{T} , and (2) search a shortest path from P_0 to P_n in graph G .

The reachability graph of a trajectory $\ddot{T}[P_0, \dots, P_n]$ w.r.t. a bound ϵ is an unweighted graph $G(V, E)$, where (1) $V = \{P_0, \dots, P_n\}$, and (2) for any nodes P_s and $P_{s+k} \in V$ ($s \geq 0, k > 0, s+k \leq n$), edge $(P_s, P_{s+k}) \in E$ if and only if the distance of each point P_{s+i} ($i \in [0, k]$) to line segment $\overrightarrow{P_s P_{s+k}}$ is not greater than ϵ .

Observe that in the reachability graph G , (1) a path from nodes P_0 to P_n is a representation of trajectory \ddot{T} . The path also reveals the subset of points of \ddot{T} used in the approximate trajectory, (2) the path length corresponds to the number of line segments in the approximate trajectory, and (3) a shortest path is an optimal representation of trajectory \ddot{T} .

Constructing the reachability graph G needs to check for all pairs of points P_s and P_{s+k} whether the distances of all points P_{s+i} ($0 < i < k$) to the line segment $\overrightarrow{P_s P_{s+k}}$ are less than ϵ . There are $O(n^2)$ pairs of points in the trajectory and checking the error of all points P_{s+i} to a line segment $\overrightarrow{P_s P_{s+k}}$ takes $O(n)$ time. Thus, the construction step takes $O(n^3)$ time. Finding shortest paths on unweighted graphs can be done in linear time. Hence, the brute-force algorithm takes $O(n^3)$ time in total.

Though the brute-force algorithm was initially developed using PED, it can be used for SED. As pointed out in [3], the construction of the reachability graph G using PED can be implemented in $O(n^2)$ time using the *sector intersection* mechanism (see Section 2.3). However, the *sector intersection* mechanism cannot work with SED. Hence, the construction of the reachability graph G using SED remains in $O(n^3)$ time, and the brute-force algorithm using SED remains in $O(n^3)$ time.

2.3 Sector Intersection based Algorithms using PED

The sector intersection (SI) algorithm [36, 40] was developed for graphic and pattern recognition in the late 1970s, for the approximation of arbitrary planar curves by linear segments or finding a polygonal approximation of a set of input data points in a 2D Cartesian coordinate system. The Sleeve algorithm [42] in the cartographic discipline essentially applies the same idea as the SI algorithm. Further, [8] optimized algorithm SI by considering the distance between a potential end point and the initial point of a line segment. It is worth

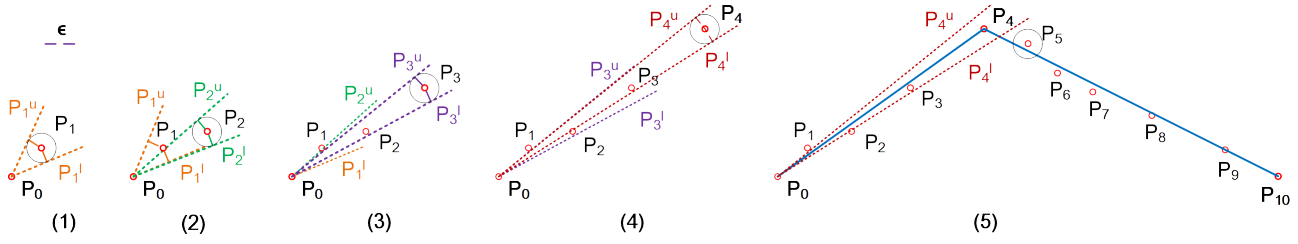


Fig. 2 Trajectory $\vec{T}[P_0, \dots, P_{10}]$ in Figure 1 is compressed into two line segments by the Sector Intersection algorithm [36, 40]. Each circle in the figure has a radius of $\epsilon/2$, which is used to define the sector.

pointing out that all these SI based algorithms use the perpendicular Euclidean distances.

Given a sequence of data points $[P_s, P_{s+1}, \dots, P_{s+k}]$ and an error bound ϵ , the SI based algorithms process the input points one by one in order, and produce a simplified polyline. Instead of using the distance threshold ϵ directly, the SI based algorithms convert the distance tolerance into a variable angle tolerance for testing the successive data points.

For the start data point P_s , any point P_{s+i} and $|\overrightarrow{P_s P_{s+i}}| > \epsilon$ ($i \in [1, k]$), there are two directed lines $\overrightarrow{P_s P_{s+i}^u}$ and $\overrightarrow{P_s P_{s+i}^l}$ such that $\text{ped}(\overrightarrow{P_{s+i}}, \overrightarrow{P_s P_{s+i}^u}) = \text{ped}(\overrightarrow{P_{s+i}}, \overrightarrow{P_s P_{s+i}^l}) = \epsilon$ and either $(\overrightarrow{P_s P_{s+i}^l} \cdot \theta < \overrightarrow{P_s P_{s+i}^u} \cdot \theta$ and $\overrightarrow{P_s P_{s+i}^u} \cdot \theta - \overrightarrow{P_s P_{s+i}^l} \cdot \theta < \pi)$ or $(\overrightarrow{P_s P_{s+i}^l} \cdot \theta > \overrightarrow{P_s P_{s+i}^u} \cdot \theta$ and $\overrightarrow{P_s P_{s+i}^u} \cdot \theta - \overrightarrow{P_s P_{s+i}^l} \cdot \theta < -\pi)$. Indeed, they form a sector $\mathcal{S}(P_s, P_{s+i}, \epsilon)$ that takes P_s as the center point and $\overrightarrow{P_s P_{s+i}^u}$ and $\overrightarrow{P_s P_{s+i}^l}$ as the border lines. Then there exists a data point Q such that for any data point P_{s+i} ($i \in [1, \dots, k]$), its perpendicular Euclidean distance to directed line $\overrightarrow{P_s Q}$ is not greater than the error bound ϵ if and only if the k sectors $\mathcal{S}(P_s, P_{s+i}, \epsilon)$ ($i \in [1, k]$) share common data points other than P_s , i.e., $\bigcap_{i=1}^k \mathcal{S}(P_s, P_{s+i}, \epsilon) \neq \{P_s\}$ [36, 40, 42].

The point Q may not belong to $\{P_s, P_{s+1}, \dots, P_{s+k}\}$. However, if P_{s+i} ($1 \leq i \leq k$) is chosen as Q , then for any data point P_{s+j} ($j \in [1, \dots, i]$), its perpendicular Euclidean distance to line segment $\overrightarrow{P_s P_{s+i}}$ is not greater than the error bound ϵ if and only if $\bigcap_{j=1}^i \mathcal{S}(P_s, P_{s+j}, \epsilon/2) \neq \{P_s\}$, as pointed out in [42].

That is, these SI based algorithms can be easily adopted for trajectory compression using PED although they have been overlooked by existing trajectory simplification studies. The SI based algorithms run in $O(n)$ time and $O(1)$ space and are one-pass algorithms.

We next illustrate how the SI based algorithms can be used for trajectory compression with an example.

Example 2 Consider Figure 2. An SI based simplification algorithm takes as input a trajectory $\vec{T}[P_0, \dots, P_{10}]$, and returns a simplified polyline consisting of two line segments $\overrightarrow{P_0 P_4}$ and $\overrightarrow{P_4 P_{10}}$. Initially, point P_0 is the start point.

(1) Point P_1 is firstly read, and the sector $\mathcal{S}(P_0, P_1, \epsilon/2)$ of P_1 is created as shown in Figure 2.(1).

(2) Then P_2 is read, and the sector $\mathcal{S}(P_0, P_2, \epsilon/2)$ is created for P_2 . The intersection of sectors $\mathcal{S}(P_0, P_1, \epsilon/2)$ and $\mathcal{S}(P_0, P_2, \epsilon/2)$ contains data points other than P_0 , which has an up border line $P_0 P_2^u$ and a low border line $P_0 P_2^l$, as shown in Figure 2.(2).

Similarly, points P_3 and P_4 are processed, as shown in Figures 2.(3) and 2.(4), respectively.

(3) When point P_5 is read, line segment $\overrightarrow{P_0 P_4}$ is produced, and point P_4 becomes the start point, as $\bigcap_{i=1}^4 \mathcal{S}(P_0, P_{s+i}, \epsilon/2) \neq \{P_0\}$ and $\bigcap_{i=1}^5 \mathcal{S}(P_0, P_{s+i}, \epsilon/2) = \{P_0\}$ as shown in Figure 2.(5).

(4) Points P_5, \dots, P_{10} are processed similarly one by one in order, and finally the algorithm outputs another line segment $\overrightarrow{P_4 P_{10}}$ as shown in Figure 2.(5). \square

However, if we use SED instead of PED, then “the k sectors $\mathcal{S}(P_s, P_{s+i}, \epsilon)$ ($i \in [1, k]$) sharing common data points other than P_s ” cannot ensure “there exists a data point Q such that for any data point P_{s+i} ($i \in [1, \dots, k]$), its **synchronized** Euclidean distance to directed line $\overrightarrow{P_s Q}$ is not greater than the error bound ϵ ”. Hence, the SI mechanism is PED specific, and not applicable for SED.

2.4 Intersection Computation of Convex Polygons

We also employ and revise a convex polygon intersection algorithm developed in [25], whose basic idea is straightforward. Assume *w.l.o.g.* that the edges of polygons \mathcal{R}_1 and \mathcal{R}_2 are oriented counterclockwise, and $\vec{A} = (P_{s_A}, P_{e_A})$ and $\vec{B} = (P_{s_B}, P_{e_B})$ are two (directed) edges on \mathcal{R}_2 and \mathcal{R}_1 , respectively.

The algorithm has \vec{A} and \vec{B} “chasing” one another, i.e., moves \vec{A} on \mathcal{R}_2 and \vec{B} on \mathcal{R}_1 counter-clockwise step by step under certain rules, so that they meet at every crossing of \mathcal{R}_1 and \mathcal{R}_2 . The rules, called *advance rules*, are carefully designed depending on geometric conditions of \vec{A} and \vec{B} . Let $\vec{A} \times \vec{B}$ be the cross product of (vectors) \vec{A} and \vec{B} , and $\mathcal{H}(\vec{A})$ be the open half-plane to the left of \vec{A} , the rules are as follows:

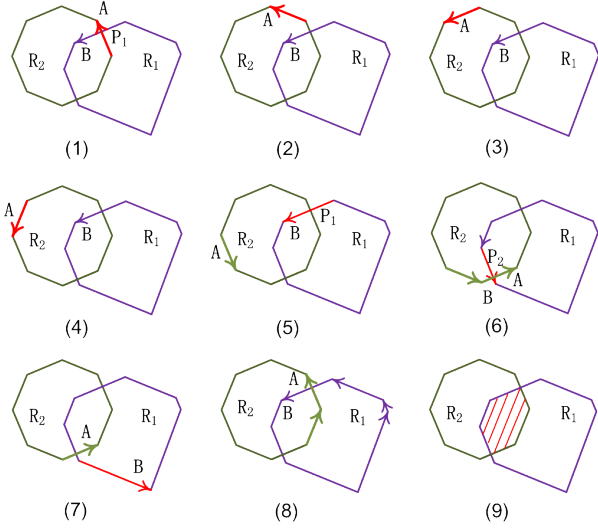


Fig. 3 A running example of convex polygon intersection.

Rule (1): If $\vec{A} \times \vec{B} < 0$ and $P_{e_A} \notin \mathcal{H}(\vec{B})$, or $\vec{A} \times \vec{B} \geq 0$ and $P_{e_B} \in \mathcal{H}(\vec{A})$, then \vec{A} is advanced a step.

For example, in Figure 3.(1) and 3.(2), \vec{A} moves forward a step as $\vec{A} \times \vec{B} > 0$ and $P_{e_B} \in \mathcal{H}(\vec{A})$.

Rule (2): If $\vec{A} \times \vec{B} \geq 0$ and $P_{e_B} \notin \mathcal{H}(\vec{A})$, or $\vec{A} \times \vec{B} < 0$ and $P_{e_A} \in \mathcal{H}(\vec{B})$, then \vec{B} is advanced a step.

For example, in Figure 3.(6) and 3.(7), \vec{B} moves forward a step as $\vec{A} \times \vec{B} < 0$ and $P_{e_A} \in \mathcal{H}(\vec{B})$.

Algorithm CPolyInter. The complete algorithm is shown in Figure 4. Given two convex polygons \mathcal{R}_1 and \mathcal{R}_2 , algorithm CPolyInter first arbitrarily sets directed edge \vec{A} on \mathcal{R}_2 and directed edge \vec{B} on \mathcal{R}_1 , respectively (line 1). It then checks the intersection of edges \vec{A} and \vec{B} . If \vec{A} intersects \vec{B} (line 3), then the algorithm checks for some special termination conditions (e.g., if \vec{A} and \vec{B} are overlapped and, at the same time, polygons \mathcal{R}_1 and \mathcal{R}_2 are on the opposite sides of the overlapped edges, then the process is terminated) (line 4), and records the inner edge, which is a boundary segment of the intersection polygon (line 5). After that, the algorithm moves on \vec{A} or \vec{B} one step under the advance rules (lines 6–11). The above processes repeated, until both \vec{A} and \vec{B} completely cycle their polygons (line 12). Next, the algorithm handles three special cases of the polygons \mathcal{R}_1 and \mathcal{R}_2 , i.e., \mathcal{R}_1 is inside of \mathcal{R}_2 , \mathcal{R}_2 is inside of \mathcal{R}_1 , and $\mathcal{R}_1 \cap \mathcal{R}_2 = \emptyset$ (line 13). At last, it returns the intersection polygon (line 14).

Example 3 Figure 3 shows a running example of the convex polygon intersection algorithm CPolyInter.

(1) Initially, directed edges \vec{A} and \vec{B} are on polygons \mathcal{R}_2 and \mathcal{R}_1 , respectively, such that $\vec{A} \cap \vec{B} = \{P_1\}$, i.e., \vec{A} and \vec{B} intersect on point P_1 , as shown in Figure 3.(1).

(2) Then, because $\vec{A} \times \vec{B} > 0$ and $P_{e_B} \in \mathcal{H}(\vec{A})$, by the advance rule (1), edge \vec{A} moves on a step and makes

Algorithm CPolyInter ($\mathcal{R}_1, \mathcal{R}_2$)

```

1. set  $\vec{A}$  and  $\vec{B}$  arbitrarily on  $\mathcal{R}_2$  and  $\mathcal{R}_1$ , respectively;
2. repeat
3.   if  $\vec{A} \cap \vec{B} \neq \emptyset$  then
4.     Check for termination;
5.     Update an inside flag;
6.     if  $(\vec{A} \times \vec{B} < 0 \text{ and } P_{e_A} \notin \mathcal{H}(\vec{B})) \text{ or}$ 
7.        $(\vec{A} \times \vec{B} \geq 0 \text{ and } P_{e_B} \in \mathcal{H}(\vec{A}))$  then
8.       advance  $\vec{A}$  one step;
9.     elseif  $(\vec{A} \times \vec{B} \geq 0 \text{ and } P_{e_B} \notin \mathcal{H}(\vec{A})) \text{ or}$ 
10.       $(\vec{A} \times \vec{B} < 0 \text{ and } P_{e_A} \in \mathcal{H}(\vec{B}))$  then
11.      advance  $\vec{B}$  one step;
12. until both  $\vec{A}$  and  $\vec{B}$  cycle their polygons
13. handle  $\mathcal{R}_1 \subset \mathcal{R}_2$  and  $\mathcal{R}_2 \subset \mathcal{R}_1$  and  $\mathcal{R}_1 \cap \mathcal{R}_2 = \emptyset$  cases;
14. return  $\mathcal{R}_1 \cap \mathcal{R}_2$ .
```

Fig. 4 Algorithm for convex polygon intersection [25].

$\vec{A} \cap \vec{B} = \emptyset$ as shown in Figure 3.(2). After 7 steps of moving of edge \vec{A} or \vec{B} , each by an advance rule, \vec{A} and \vec{B} intersect on P_2 , as shown in Figure 3.(6).

(3) Next, because $\vec{A} \times \vec{B} < 0$ and $P_{e_A} \in \mathcal{H}(\vec{B})$, by the advance rule (2), edge \vec{B} moves on a step, and makes $\vec{A} \cap \vec{B} = \emptyset$, as shown in Figure 3.(7).

(4) After 6 steps of moving of edge \vec{B} or \vec{A} one by one, both edges \vec{A} and \vec{B} have finished their cycles as shown in Figure 3.(8).

(5) The algorithm finally returns the intersection polygon as shown in Figure 3.(9). \square

Algorithm CPolyInter has a time complexity of $O(|\mathcal{R}_1| + |\mathcal{R}_2|)$, where $|\mathcal{R}|$ is the number of edges of polygon \mathcal{R} . It is also worth pointing out that $|\mathcal{R}_1 \cap \mathcal{R}_2| \leq (|\mathcal{R}_1| + |\mathcal{R}_2|)$.

3 Local Synchronous Distance Checking

In this section, we develop a local synchronous distance checking approach, lay down the key for the one-pass trajectory simplification algorithms using SED (Section 4), such that each point in a trajectory is checked only once in $O(1)$ time during the entire process of trajectory simplification. The key the local synchronous distance checking method lies in a new concept of spatio-temporal cones that converts the SED distance tolerance into the intersection of spatio-temporal cones for testing the successive data points. More specifically, we first substantially extend the sectors in Section 2.3 from a 2D space to a spatio-temporal 3D space, which leads to spatio-temporal cones. Then we prove that the SED distance checking can be achieved by the intersection of spatio-temporal cones. Finally, we simplify the spatio-temporal cone intersection into the circle intersection, and approximate scircle with a special class of (fixed rotation and edge number) polygons.

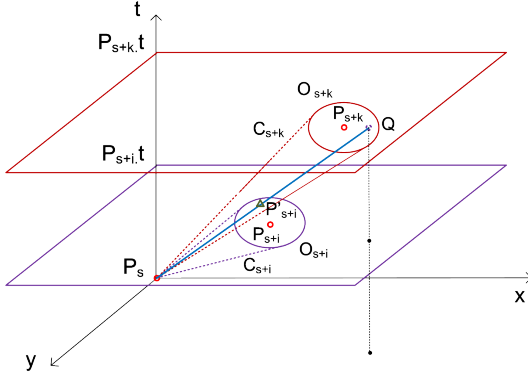


Fig. 5 Examples of spatio-temporal cones in a 3D Cartesian coordinate system, where (1) P_s , P_{s+i} and P_{s+k} are three points, (2) O_{s+i} and O_{s+k} are two synchronous circles, (3) C_{s+i} and C_{s+k} are two spatio-temporal cones, (4) Q is a point in synchronous circle O_{s+k} , and (5) P'_{s+i} is the intersection point of line $\overrightarrow{P_s Q}$ and synchronous circle O_{s+i} .

We consider a sub-trajectory $\ddot{\mathcal{T}}_s[P_s, \dots, P_{s+k}]$, an error bound ϵ , and a 3D Cartesian coordinate system whose origin, x -axis, y -axis and t -axis are P_s , longitude, latitude and time, respectively.

3.1 Spatio-Temporal Cone Intersection

We first present the *spatio-temporal cone intersection* method in a 3D Cartesian coordinate system.

Synchronous Circles (\mathcal{O}). The synchronous circle of a data point P_{s+i} ($1 \leq i \leq k$) in $\ddot{\mathcal{T}}_s$ w.r.t. an error bound ϵ , denoted as $\mathcal{O}(P_{s+i}, \epsilon)$, or O_{s+i} in short, is a circle on the plane $P.t - P_{s+i}.t = 0$ such that P_{s+i} is its center and ϵ is its radius.

Spatio-temporal cones (\mathcal{C}). Given a start point P_s of $\ddot{\mathcal{T}}_s$ and an error bound ϵ , the spatio-temporal cone (or simply *cone*) of a data point P_{s+i} ($1 \leq i \leq k$) in $\ddot{\mathcal{T}}_s$ w.r.t. P_s and ϵ , denoted as $\mathcal{C}(P_s, \mathcal{O}(P_{s+i}, \epsilon))$, or C_{s+i} in short, is an oblique circular cone such that point P_s is its apex and the synchronous circle $\mathcal{O}(P_{s+i}, \epsilon)$ of point P_{s+i} is its base.

Example 4 (1) Figure 5 shows two synchronous circles, $\mathcal{O}(P_{s+i}, \epsilon)$ of point P_{s+i} and $\mathcal{O}(P_{s+k}, \epsilon)$ of point P_{s+k} . It is easy to see that for any point in the area of a circle $\mathcal{O}(P_{s+i}, \epsilon)$, its distance to P_{s+i} is not greater than ϵ .

(2) Figure 5 also illustrates two example spatio-temporal cones: $\mathcal{C}(P_s, \mathcal{O}(P_{s+i}, \epsilon))$ (purple) and $\mathcal{C}(P_s, \mathcal{O}(P_{s+k}, \epsilon))$ (red), with the same apex P_s and error bound ϵ . \square

Indeed, the SED distance tolerance can be checked by finding the common intersection of spatio-temporal cones, as shown below.

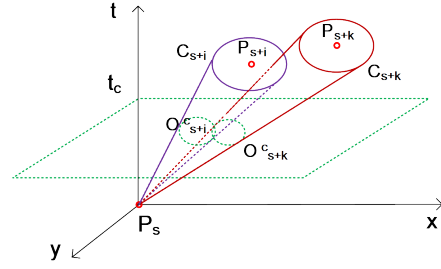


Fig. 6 Cone projection circles.

Proposition 1: Given a sub-trajectory $[P_s, \dots, P_{s+k}]$ and an error bound ϵ , there exists a point Q such that $Q.t = P_{s+k}.t$ and $\text{sed}(P_{s+i}, \overrightarrow{P_s Q}) \leq \epsilon$ for each $i \in [1, k]$ if and only if $\bigcap_{i=1}^k \mathcal{C}(P_s, \mathcal{O}(P_{s+i}, \epsilon)) \neq \{P_s\}$. \square

By Proposition 1, we now have a spatio-temporal cone intersection method in a 3D Cartesian coordinate system, which significantly extends the sector intersection method [36, 40, 42] from a 2D space to a spatio-temporal 3D space.

3.2 Circle Intersection

For spatio-temporal cones with the same apex P_s , we then show that the checking of their intersection can be computed by a much simpler way, i.e., the checking of intersection of cone projection circles on a plane.

Cone projection circles. The projection of a cone $\mathcal{C}(P_s, \mathcal{O}(P_{s+i}, \epsilon))$ on a plane $P.t - t_c = 0$ ($t_c > P_s.t$) is a circle $\mathcal{O}^c(P_{s+i}^c, r_{s+i}^c)$, or O_{s+i}^c in short, such that (1) $P_{s+i}^c.x = P_s.x + w \cdot (P_{s+i}.x - P_s.x)$, (2) $P_{s+i}^c.y = P_s.y + w \cdot (P_{s+i}.y - P_s.y)$, (3) $P_{s+i}^c.t = t_c$, and (4) $r_{s+i}^c = w \cdot \epsilon$, where $w = \frac{t_c - P_s.t}{P_{s+i}.t - P_s.t}$.

Recall that the base of a cone $\mathcal{C}(P_s, \mathcal{O}(P_{s+i}, \epsilon))$ is a circle on plane $P.t - P_{s+i}.t = 0$, and plane $P.t - t_c = 0$ is parallel to plane $P.t - P_{s+i}.t = 0$. These ensure that the projection a cone on plane $P.t - t_c = 0$ is a circle.

Example 5 In Figure 6, the green dashed circles $\mathcal{O}^c(P_{s+i}^c, r_{s+i}^c)$ and $\mathcal{O}^c(P_{s+k}^c, r_{s+k}^c)$ on plane “ $P.t - t_c = 0$ ” are the projection circles of cones $\mathcal{C}(P_s, \mathcal{O}(P_{s+i}, \epsilon))$ and $\mathcal{C}(P_s, \mathcal{O}(P_{s+k}, \epsilon))$ on the plane. \square

Proposition 2: Given a sub-trajectory $[P_s, \dots, P_{s+k}]$, an error bound ϵ , and any $t_c > P_s.t$, there exists a point Q such that $Q.t = P_{s+k}.t$ and $\text{sed}(P_{s+i}, \overrightarrow{P_s Q}) \leq \epsilon$ for all points P_{s+i} ($i \in [1, k]$) if and only if $\bigcap_{i=1}^k \mathcal{O}^c(P_{s+i}^c, r_{s+i}^c) \neq \emptyset$. \square

Proposition 2 tells us that the intersection checking of spatio-temporal cones can be reduced to simply check the intersection of cone projection circles on a plane.

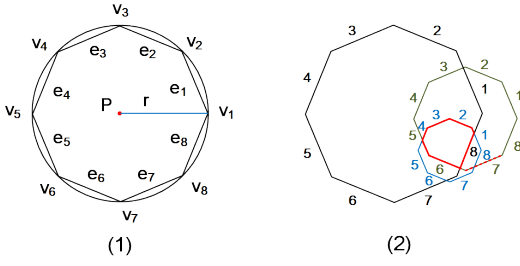


Fig. 7 Regular octagons and their intersections ($m = 8$).

3.3 Inscribed Regular Polygon Intersection

Finding the common intersection of n circles on a plane has a time complexity of $O(n \log n)$ [34], which cannot be used for designing one-pass trajectory simplification algorithms using SED. Intuitively, we can approximate a circle with its m -edges inscribed polygon whose intersection can be computed much faster. However, the intersection of two general m -edges polygons may produce a polygon with more than m edges, thus, the time complexity of finding the common intersection of n polygons on a plane is not linear. To solve this problem, we approximate a circle with a fixed rotation and m -edges inscribed regular polygon.

Inscribed regular polygons (\mathcal{R}). Given a cone projection circle $\mathcal{O}^c(P, r)$, its inscribed m -edges regular polygon is denoted as $\mathcal{R}(V, E)$, where (1) $V = \{v_1, \dots, v_m\}$ is the set of vertexes that are defined by a polar coordinate system, whose origin is the center P of \mathcal{O}^c , as follows:

$$v_j = (r, \frac{(j-1)}{m}2\pi), j \in [1, m],$$

and (2) $E = \{\overrightarrow{v_m v_1}\} \cup \{\overrightarrow{v_j v_{j+1}} \mid j \in [1, m-1]\}$ is the set of edges that are labeled with the subscript of their start points. Figure 7.(1) illustrates the inscribed regular octagon ($m = 8$) of a cone projection circle $\mathcal{O}^c(P, r)$.

Let \mathcal{R}_{s+i} ($1 \leq i \leq k$) be the inscribed regular polygon of the cone projection circle $\mathcal{O}^c(P_{s+i}^c, r_{s+i}^c)$, \mathcal{R}_l^* ($1 \leq l \leq k$) be the intersection $\bigcap_{i=1}^l \mathcal{R}_{s+i}$, and E^j ($1 \leq j \leq m$) be the group of k edges labeled with j in all \mathcal{R}_{s+i} ($i \in [1, k]$). It is easy to verify that all edges in all \mathcal{R}_{s+i} are in parallel (or overlapping) with each other by the above definition of inscribed regular polygons, as illustrated in Figure 7.(2).

The intersection of inscribed regular polygons holds a nice property, as shown below.

Proposition 3: The intersection $\mathcal{R}_l^* \cap \mathcal{R}_{s+l+1}$ ($1 \leq l < k$) has at most m edges, i.e., at most one from each edge group.

Figure 7.(2) shows the intersection polygon (red lines) of \mathcal{R}_1 , \mathcal{R}_2 and \mathcal{R}_3 with 7 edges, and here edges labeled with 7 have no contributions to the resulting intersection polygon.

Based on Proposition 3, we also have the following.

Proposition 4: The intersection of \mathcal{R}_l^* and \mathcal{R}_{s+l+1} ($1 \leq l < k$) can be done in $O(1)$ time.

By Proposition 4, we have a local synchronous distance checking method.

3.4 Speedup Inscribed Regular Polygon Intersection

Recall that the intersection of inscribed regular polygons can be computed by the convex polygon intersection algorithm CPolyInter [25] in Figure 4. However, observe that algorithm CPolyInter is for general convex polygons, while the inscribed regular polygons \mathcal{R}_{s+i} ($i \in [1, k]$) of the cone projection circles are constructed in a unified way, i.e., fixed rotation and edge number, which allows us to develop a faster method to speed up the computation of their intersection.

We next explain the key idea for speeding up the computation. Observe that when the edges $\vec{A} = (P_{s_A}, P_{e_A})$ and $\vec{B} = (P_{s_B}, P_{e_B})$ on polygons \mathcal{R}_2 and \mathcal{R}_1 (both \mathcal{R}_2 and \mathcal{R}_1 can be either inscribed regular polygons or the common intersection of inscribed regular polygons) are “chasing” one another as the way the convex polygon intersection algorithm CPolyInter does, every segment in the two polygons being intersected has to originate from one of the m edges of the regular polygons and the geometric similarity of the regular polygons, we may advance edge \vec{A} or \vec{B} multiple steps at a time, instead of a single step at a time of the convex polygon intersection algorithm CPolyInter. For example, in Figure 3.(1)–(5), edge \vec{A} successively moves four steps, each under the advance rule (1) “ $(\vec{A} \times \vec{B} < 0$ and $P_{e_A} \notin \mathcal{H}(\vec{B}))$ or $(\vec{A} \times \vec{B} \geq 0$ and $P_{e_B} \in \mathcal{H}(\vec{A}))$ ” of algorithm CPolyInter. Alternatively, we can directly move A from Figure 3.(1) to Figure 3.(5), by reducing four steps to one step only. To achieve this, we first develop two extra advance rules (Propositions 5 and 6) for the intersection of inscribed regular polygons.

Proposition 5: If either $(\vec{A} \cap \vec{B} \neq \emptyset$ and $\vec{A} \times \vec{B} < 0$ and $P_{e_A} \notin \mathcal{H}(\vec{B}))$ or $(\vec{A} \cap \vec{B} \neq \emptyset$ and $\vec{A} \times \vec{B} \geq 0$ and $P_{e_B} \in \mathcal{H}(\vec{A}))$ holds, then \vec{A} advances s steps such that

$$s = \begin{cases} 2 \times (g(\vec{B}) - g(\vec{A})) & \text{if } g(\vec{B}) > g(\vec{A}) \\ 1 & \text{if } g(\vec{A}) = g(\vec{B}) \\ 2 \times (m + g(\vec{B}) - g(\vec{A})) & \text{if } g(\vec{B}) < g(\vec{A}), \end{cases}$$

in which $g(e)$ denotes the label of edge e .

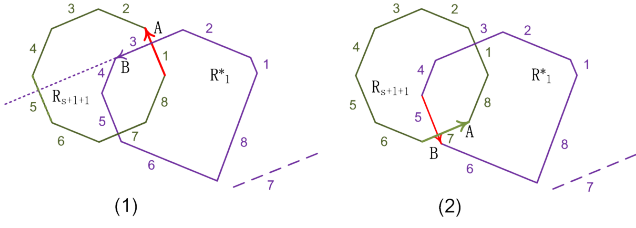


Fig. 8 Examples of fast advancing rules.

We next explain how the edge \vec{A} advances based on Proposition 5. Indeed, \vec{A} is moved from its original position to its symmetric edge on \mathcal{R}_{s+l+1} w.r.t. the symmetric line that is perpendicular to \vec{B} on \mathcal{R}_l^* . For example, in Figure 8.(1), there is $\vec{A} \cap \vec{B} \neq \emptyset$ and $\vec{A} \times \vec{B} \geq 0$ and $P_{e_B} \in \mathcal{H}(\vec{A})$, hence \vec{A} moves on. As $g(\vec{B}) = 3 > 1 = g(\vec{A})$, \vec{A} moves forward $2 \times (g(\vec{B}) - g(\vec{A})) = 2 \times (3 - 1) = 4$ steps. Here, the label of edge \vec{A} is changed to 5, its symmetric edge 1 on \mathcal{R}_{s+l+1} w.r.t. the symmetric line that is perpendicular to \vec{B} labeled with 3 on \mathcal{R}_l^* .

Proposition 6: If either $(\vec{A} \cap \vec{B} \neq \emptyset \text{ and } \vec{A} \times \vec{B} \geq 0 \text{ and } P_{e_B} \notin \mathcal{H}(\vec{A}))$ or $(\vec{A} \cap \vec{B} \neq \emptyset \text{ and } \vec{A} \times \vec{B} < 0 \text{ and } P_{e_A} \in \mathcal{H}(\vec{B}))$ holds, then edge \vec{B} is directly moved to the edge after the one having the same edge group as edge \vec{A} . \square

We next explain how the edge \vec{B} advances based on Proposition 6. For example, in Figure 8.(2), $\vec{A} \cap \vec{B} \neq \emptyset$ and $\vec{A} \times \vec{B} < 0$ and $P_{e_A} \in \mathcal{H}(\vec{B})$, hence \vec{B} is moved forward. As the edge \vec{A} is labeled with 7, \vec{B} moves to the edge labeled with 8 on \mathcal{R}_l^* , which is the next of the edge labeled with 7 on \mathcal{R}_l^* . Note that if the edge labeled with 8 did not actually exist in the intersection polygon \mathcal{R}_l^* , then \vec{B} should repeatedly move on until it reaches the first “real” edge on \mathcal{R}_l^* .

We then present our faster algorithm for computing the intersection of inscribed regular polygons that makes of the advance rules in terms of Propositions 5 and 6.

Algorithm FastRPolyInter. The regular polygon intersection algorithm, i.e., FastRPolyInter, is the optimized version of the convex polygon intersection algorithm CPolyInter, based on Propositions 5 and 6. We also save vertexes of a polygon in a fixed size array, which is different from CPolyInter that saves polygons in linked lists. Considering the regular polygons each having a fixed number of vertexes/edges, marked from 1 to m , this policy allows us to quickly address an edge or a vertex with its label.

Given intersection polygon \mathcal{R}_l^* of the preview l polygons and the next approximate polygon \mathcal{R}_{s+l+1} , the algorithm FastRPolyInter returns $\mathcal{R}_{l+1}^* = \mathcal{R}_l^* \cap \mathcal{R}_{s+l+1}$.

It runs the similar routine as the CPolyInter algorithm, except that (1) it saves polygons in arrays, and (2) the advance strategies are partitioned into two parts, i.e., $\vec{A} \cap \vec{B} \neq \emptyset$ and $\vec{A} \cap \vec{B} = \emptyset$, where the former applies Propositions 5 and 6, and the latter remains the same as algorithm CPolyInter.

Correctness and complexity analyses. Observe that algorithm FastRPolyInter basically has the same routine as algorithm CPolyInter, except that it speeds up the advance of directed edges \vec{A} and \vec{B} under certain circumstances as shown by Propositions 5 and 6, which together ensure the correctness of FastRPolyInter. Moreover, algorithm FastRPolyInter runs in $O(1)$ time by Proposition 4.

4 One-Pass Trajectory Simplification

Following [15, 39], we consider two classes of trajectory simplification. The first one, referred to as *strong simplification*, that takes as input a trajectory \vec{T} , an error bound ϵ and the number m of edges for inscribed regular polygons, and produces a simplified trajectory \vec{T}' such that all data points in \vec{T}' belong to \vec{T} . The second one, referred to as *weak simplification*, that takes as input a trajectory \vec{T} , an error bound ϵ and the number m of edges for inscribed regular polygons, and produces a simplified trajectory \vec{T}' such that some data points in \vec{T}' may not belong to \vec{T} . That is, weak simplification allows data interpolation. The main result here is stated as follows.

Theorem 7 *There exist one-pass, error bounded and strong and weak trajectory simplification algorithms using the synchronous Euclidean distance (SED).*

We shall prove this by providing such algorithms for both strong and weak trajectory simplifications, by employing the synchronous distance checking technique developed in Section 3.

4.1 Strong Trajectory Simplification

Recall that in Propositions 1 and 2, the point Q may not be in the input sub-trajectory $[P_s, \dots, P_{s+k}]$. If we restrict $Q = P_{s+k}$, the end point of the sub-trajectory, then the narrow cones whose base circles with a radius of $\epsilon/2$ suffice, as shown below.

Proposition 8: *Given a sub-trajectory $[P_s, \dots, P_{s+k}]$ and an error bound ϵ , $\text{sed}(P_{s+i}, P_{s+k}) \leq \epsilon$ for each $i \in [1, k]$ if $\bigcap_{i=1}^k \mathcal{C}(P_s, \mathcal{O}(P_{s+i}, \epsilon/2)) \neq \{P_s\}$. \square*

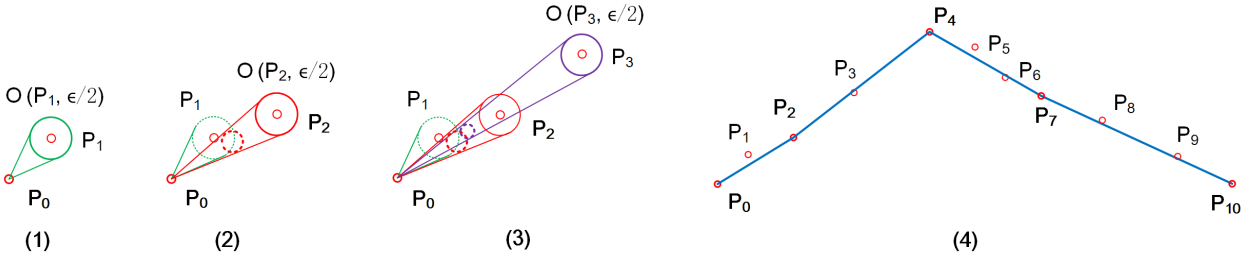


Fig. 9 A running example of the CISED-S algorithm. The points and the oblique circular cones are projected on an x-y space. The trajectory $\vec{T}[P_0, \dots, P_{10}]$ is compressed into four line segments. The solid line circles are *synchronous circles*, each has a radius of $\epsilon/2$, and the dash line circles are *cone projection circles* whose inscribed regular polygons are computed.

We now present the one-pass error bounded *strong trajectory simplification* algorithm using SED by Proposition 8, as shown in Figure 10.

Procedure getRegularPolygon. We first present procedure `getRegularPolygon` that, given a cone projection circle, generates its inscribed m -edges regular polygon, following the definition in Section 3.3.

The parameters P_s, P_i, r and t_c together form the projection circle $\mathcal{O}^c(P_i^c, r_i^c)$ of the spatio-temporal cone $\mathcal{C}(P_s, \mathcal{O}(P_i, r))$ of point P_i w.r.t. point P_s on the plane $P.t - t_c = 0$. Firstly, $P_i^c.x$ and $P_i^c.y$ are computed (lines 1–3), and $r_i^c = w \cdot r$. Then it builds and returns an m -edges inscribed regular polygon \mathcal{R} of $\mathcal{O}^c(P_i^c, r_i^c)$ (lines 4–8), by transforming a polar coordinate system into a Cartesian one. Note here $\theta, r \cdot \sin \theta$ and $r \cdot \cos \theta$ only need to be computed once during the entire processing of a trajectory.

Algorithm CISED-S. It takes as input a trajectory $\vec{T}[P_0, \dots, P_n]$, an error bound ϵ and the number m of edges for inscribed regular polygons, and returns a simplified trajectory \bar{T} of \vec{T} .

The algorithm first initializes the start point P_s to P_0 , the index i of the current data point to 1, the intersection polygon \mathcal{R}^* to \emptyset , the output \bar{T} to \emptyset , and t_c to $P_1.t$, respectively (line 1). The algorithm sequentially processes the data points of the trajectory one by one (lines 2–10). It gets the m -edges inscribed regular polygon w.r.t. the current point P_i (line 3) by calling procedure `getRegularPolygon`. When $\mathcal{R}^* = \emptyset$, the intersection polygon \mathcal{R}^* is simply initialized as \mathcal{R} (lines 4, 5). Otherwise, \mathcal{R}^* is the intersection of the current regular polygon \mathcal{R} with \mathcal{R}^* by calling procedure `FastRPolyInter()` introduced in Section 3.4 (line 7). If the resulting intersection \mathcal{R}^* is empty, then a new line segment $\overrightarrow{P_s P_{i-1}}$ is generated (lines 8–10). The process repeats until all points have been processed (line 11). After the final line segment $\overrightarrow{P_s P_n}$ is generated (line 12), it returns the simplified piece-wise line representation \bar{T} (line 13).

Example 6 Figure 9 shows a running example of CISED-S for compressing the trajectory \vec{T} in Figure 1.

Algorithm CISED-S ($\vec{T}[P_0, \dots, P_n], \epsilon, m$)

```

1.  $P_s := P_0; i := 1; \mathcal{R}^* := \emptyset; \bar{T} := \emptyset; t_c := P_1.t;$ 
2. while  $i \leq n$  do
3.    $\mathcal{R} := \text{getRegularPolygon}(P_s, P_i, \epsilon/2, m, t_c);$ 
4.   if  $\mathcal{R}^* = \emptyset$  then /*  $\mathcal{R}^*$  needs to be initialized */
5.      $\mathcal{R}^* := \mathcal{R};$ 
6.   else
7.      $\mathcal{R}^* := \text{FastRPolyInter}(\mathcal{R}^*, \mathcal{R});$ 
8.     if  $\mathcal{R}^* = \emptyset$  then /* generate a new line segment */
9.        $i := i - 1; \bar{T} := \bar{T} \cup \{\overrightarrow{P_s P_i}\};$ 
10.       $P_s := P_i; t_c := P_{i+1}.t;$ 
11.     $i := i + 1;$ 
12.   $\bar{T} := \bar{T} \cup \{\overrightarrow{P_s P_n}\};$ 
13. return  $\bar{T}.$ 

```

Procedure getRegularPolygon (P_s, P_i, r, m, t_c)

```

1.  $w := (t_c - t_s) / (P_i.t - P_s.t);$ 
2.  $x := P_s.x + w \cdot (P_i.x - P_s.x);$ 
3.  $y := P_s.y + w \cdot (P_i.y - P_s.y);$ 
4. for ( $j := 1; j \leq m; j++$ ) do
5.    $\theta := (2j + 1) \cdot \pi / m;$ 
6.    $\mathcal{R}.v_j.x := x + w \cdot r \cdot \cos \theta;$ 
7.    $\mathcal{R}.v_j.y := y + w \cdot r \cdot \sin \theta;$ 
8. return  $\mathcal{R}.$ 

```

Fig. 10 One-pass strong trajectory simplification algorithm.

(1) After initialization, the CISED-S algorithm reads point P_1 and builds a narrow cone $\mathcal{C}(P_0, \mathcal{O}(P_1, \epsilon/2))$, taking P_0 as its apex and $\mathcal{O}(P_1, \epsilon/2)$ as its base (green dash circle). The cone is projected on the plane $P.t - P_1.t = 0$, and the inscribed regular polygon \mathcal{R}_1 of the projection circle is returned. As \mathcal{R}^* is empty, \mathcal{R}^* is set to \mathcal{R}_1 .

(2) The algorithm reads P_2 and builds $\mathcal{C}(P_0, \mathcal{O}(P_2, \epsilon/2))$ (red dash circle). The cone is also projected on the plane $P.t - P_1.t = 0$ and the inscribed regular polygon \mathcal{R}_2 of the projection circle is returned. As $\mathcal{R}^* = \mathcal{R}_1$ is not empty, \mathcal{R}^* is set to the intersection of \mathcal{R}_2 and \mathcal{R}^* , which is $\mathcal{R}_1 \cap \mathcal{R}_2 \neq \emptyset$.

(3) For point P_3 , the algorithm runs the same routine as P_2 until the intersection of \mathcal{R}_3 and \mathcal{R}^* is \emptyset . Thus, a line segment $\overrightarrow{P_0 P_2}$ is generated, and the process of a new line segment is started, taking P_2 as the new start point and $P.t - P_3.t = 0$ as the new projection plane.

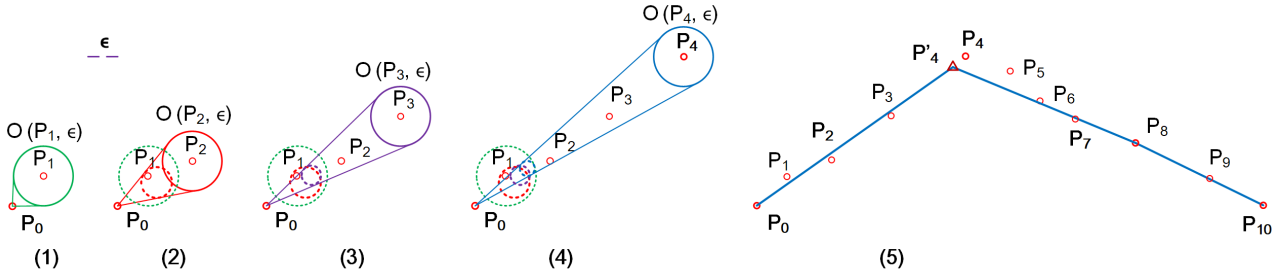


Fig. 11 A running example of the CISED-W algorithm. The points and the oblique circular cones are projected on an x-y space. The trajectory $\ddot{T}[P_0, \dots, P_{10}]$ is compressed into three line segments. The solid line circles are *synchronous circles*, each has a radius of ϵ , and the dash line circles are *cone projection circles*. Note in (5) a point, P'_4 , is interpolated.

(4) At last, the algorithm outputs four continuous line segments, *i.e.*, $\{\overrightarrow{P_0P_2}, \overrightarrow{P_2P_4}, \overrightarrow{P_4P_7}, \overrightarrow{P_7P_{10}}\}$. \square

4.2 Weak Trajectory Simplification

We then present the one-pass error bounded *weak simplification* algorithm using SED. By allowing data interpolations, it extends the radius of the base circles of spatio-temporal cones in CISED-S from $\epsilon/2$ to ϵ , which leads to better compression ratios than CISED-S. Recall that in Proposition 2, the point Q may not be in the input sub-trajectory $[P_s, \dots, P_{s+k}]$, which can be treated as an interpolated data point.

Algorithm CISED-W. Given a trajectory $\ddot{T}[P_0, \dots, P_n]$, an error bound ϵ and the number m of edges for inscribed regular polygons, it returns a simplified trajectory, which may contain interpolated points. By Proposition 2, algorithm CISED-W generates spatio-temporal cones whose bases are circles with a radius of ϵ , and, hence, it replaces $\epsilon/2$ with ϵ (line 3 of CISED-S). It also generates new line segments with data points Q (may be interpolated points), and, hence, it replaces point P_i and line segment $\overrightarrow{P_sP_i}$ (lines 9 and 10 of algorithm CISED-S) with Q and $\overrightarrow{P_sQ}$, respectively, such that Q is generated as follows.

Proposition 9: Given a sub-trajectory $\ddot{T}[P_s, \dots, P_{s+k}]$ and an error bound ϵ , $t_c = P_{s+k}.t$ and \mathcal{R}_k^* be the intersection of all polygons \mathcal{R}_{s+i} ($i \in [1, k]$) on the plane $P.t - t_c = 0$. If \mathcal{R}_k^* is not empty, then any point in the area of \mathcal{R}_k^* is feasible for Q . \square

The choice of a point Q from \mathcal{R}_k^* may slightly affect the compression ratios and average errors. However, the choice of an optimal Q is non-trivial. For the benefit of running time, we apply the following strategies.

- (1) If P_{s+k} is in the area of \mathcal{R}_k^* w.r.t. $t_c = P_{s+k}.t$, then Q is simply set to P_{s+k} .
- (2) If $\mathcal{R}_k^* \neq \emptyset$ and P_{s+k} is not in the area of \mathcal{R}_k^* w.r.t. $t_c = P_{s+k}.t$, then the central point of \mathcal{R}_k^* is chosen as Q .

(3) If $t_c \neq P_{s+k}.t$, which is the general case, then we project the intersection polygon \mathcal{R}_k^* w.r.t. $t_c \neq P_{s+k}.t$ on the plane $P.t - P_{s+k}.t = 0$, and apply strategies (1) and (2) above. That is, the projection has no effects on the choice of Q .

Example 7 Figure 11 shows a running example of algorithm CISED-W for compressing the trajectory \ddot{T} in Figure 1 again.

- (1) After initialization, algorithm CISED-W reads point P_1 and builds an *oblique circular cone* $\mathcal{C}(P_0, \mathcal{O}(P_1, \epsilon))$, and projects it on the plane $P.t - P_1.t = 0$. The inscribed regular polygon \mathcal{R}_1 of the projection circle is returned and the intersection \mathcal{R}^* is set to \mathcal{R}_1 .
- (2) P_2 , P_3 and P_4 are processed in turn. The intersection polygons \mathcal{R}^* are not empty.
- (3) For point P_5 , the intersection of polygons \mathcal{R}_5 and \mathcal{R}^* is \emptyset . Thus, line segment $\overrightarrow{P_0Q} = \overrightarrow{P_0P'_4}$ is output, and a new line segment is started such that point $Q = P'_4$ is the new start point and plane $P.t - P_5.t = 0$ is the new projection plane.
- (4) At last, the algorithm outputs 3 continuous line segments, *i.e.*, $\overrightarrow{P_0P'_4}$, $\overrightarrow{P'_4P_8}$ and $\overrightarrow{P_8P_{10}}$, in which P'_4 is an interpolated data point not in \ddot{T} . \square

Correctness and complexity analyses. The correctness of algorithms CISED-S and CISED-W follows from Propositions 2 and 8, and Propositions 2 and 9, respectively. It is easy to verify that each data point in a trajectory is only processed once, and each can be done in $O(1)$ time, as both procedures `getRegularPolygon` and `FastRPolyInter` can be done in $O(1)$ time. Hence, these algorithms are both one-pass error bounded trajectory simplification algorithms. It is also easy to see that these algorithms take $O(1)$ space.

5 Experimental Study

In this section, we present an extensive experimental study of our one-pass trajectory simplification al-

Table 2 Real-life trajectory datasets

Data Sets	Number of Trajectories	Sampling Rates (s)	Points Per Trajectory (K)	Total points
ServiceCar	1,000	3-5	~ 114.0	114M
GeoLife	182	1-5	~ 131.4	24.2M
Mopsi	51	2	~ 153.9	7.9M
PrivateCar	10	1	~ 11.8	112.8K

gorithms (CISED-S and CISED-W) compared with the optimal algorithm using SED and existing algorithms of DPSED and SQUISH-E on trajectory datasets. Using four real-life trajectory datasets, we conducted four sets of experiments to evaluate: (1) the compression ratios of algorithms CISED-S and CISED-W vs. DPSED, SQUISH-E and the optimal algorithm, (2) the average errors of algorithms CISED-S and CISED-W vs. DPSED, SQUISH-E and the optimal algorithm, (3) the running time of algorithms CISED-S and CISED-W vs. DPSED, SQUISH-E and the optimal algorithm, (4) the impacts of polygon intersection algorithms FastRPolyInter and CPolyInter and the edge number m of inscribed regular polygons to the compression ratios, errors and running time of algorithms CISED-S and CISED-W, and (5) the impacts of the distance metrics PED and SED on the compression ratios, errors and running time of trajectory simplification algorithms.

5.1 Experimental Setting

Real-life Trajectory Datasets. We use four real-life datasets ServiceCar, GeoLife, Mopsi and PrivateCar shown in Table 2 to test our solutions.

(1) *Service car trajectory data* (ServiceCar) is the GPS trajectories collected by a Chinese car rental company during Apr. 2015 to Nov. 2015. The sampling rate was one point per 3–5 seconds, and each trajectory has around 114.1K points.

(2) *GeoLife trajectory data* (GeoLife) is the GPS trajectories collected in GeoLife project [43] by 182 users in a period from Apr. 2007 to Oct. 2011. These trajectories have a variety of sampling rates, among which 91% are logged in each 1-5 seconds per point.

(3) *Mopsi trajectory data* (Mopsi) is the GPS trajectories collected in Mopsi project [1] by 51 users in a period from 2008 to 2014. Most routes are in Joensuu region, Finland. The sampling rate was one point per 2 seconds, and each trajectory has around 153.9K points.

(4) *Private car trajectory data* (PrivateCar) is a small set GPS trajectories collected with a high sampling rate of one point per second by our team members in 2017. There are 10 trajectories and each trajectory has around 11.8K points.

As the optimal LS algorithm [14] it has both high time and space complexities, *i.e.*, $O(n^3)$ time and $O(n^2)$ space, it is impossible to compress the entire datasets (too slow and out of memory). Hence, we further build four *small datasets*, each dataset includes 10 middle-size (10K points per trajectory) trajectories selected from ServiceCar, GeoLife, Mopsi and PrivateCar, respectively.

Algorithms and implementation. We implement seven LS algorithms, *i.e.*, our CISED-S and CISED-W, sector intersection algorithm using PED (SIPED) [8,42], DPPED [7] and DPSED [20] (the existing sub-optimal LS algorithms having the best compression ratios), SQUISH-E [23] (the fastest existing LS algorithm using SED) and the optimal LS algorithm using SED (see Section 2.2). We also implement the polygon intersection algorithms, CPolyInter and our FastRPolyInter.

All algorithms were implemented with Java. All tests were run on an x64-based PC with 8 Intel(R) Core(TM) i7-6700 CPU @ 3.40GHz and 8GB of memory, and each test was repeated over 3 times and the average is reported here.

5.2 Experimental Results

We next present our findings.

5.2.1 Evaluation of Compression Ratios

In the first set of tests, we evaluate the impacts of parameter m on the compression ratios of our algorithms CISED-S and CISED-W, and compare the compression ratios of CISED-S and CISED-W with DPSED, SQUISH-E and the optimal algorithm. The compression ratio is defined as follows: Given a set of trajectories $\{\ddot{\mathcal{T}}_1, \dots, \ddot{\mathcal{T}}_M\}$ and their piece-wise line representations $\{\overline{\mathcal{T}}_1, \dots, \overline{\mathcal{T}}_M\}$, the compression ratio of an algorithm is $(\sum_{j=1}^M |\overline{\mathcal{T}}_j|) / (\sum_{j=1}^M |\ddot{\mathcal{T}}_j|)$. By the definition, *algorithms with lower compression ratios are better.*

Exp-1.1: Impacts of parameter m on compression ratios. To evaluate the impacts of the number m of edges of polygons on the compression ratios of algorithms CISED-S and CISED-W, and also to confirm that our fast regular polygon intersection algorithm FastRPolyInter has the same compression ratios as the convex polygon intersection algorithm CPolyInter, we

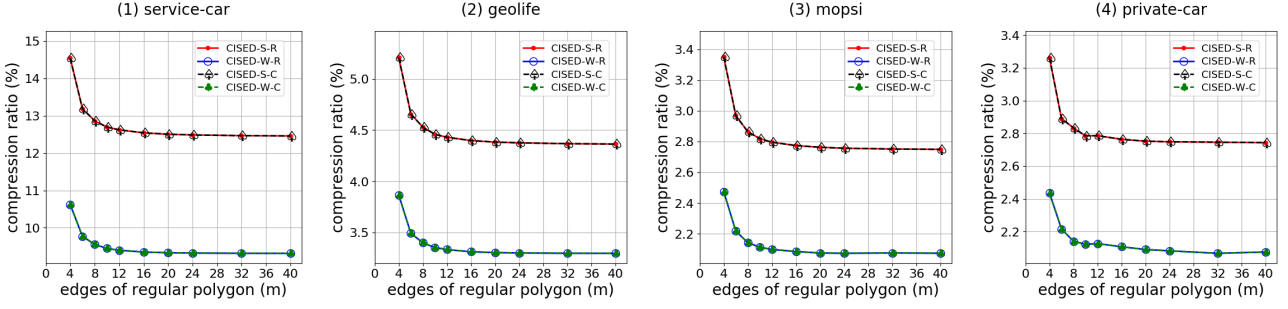


Fig. 12 Evaluation of compression ratios: fixed error bound with $\epsilon = 60$ meters and varying m . Here “R” denotes our fast regular polygon intersection algorithm FastRPolyInter, and “C” denotes the convex polygon intersection algorithm CPolyInter, respectively.

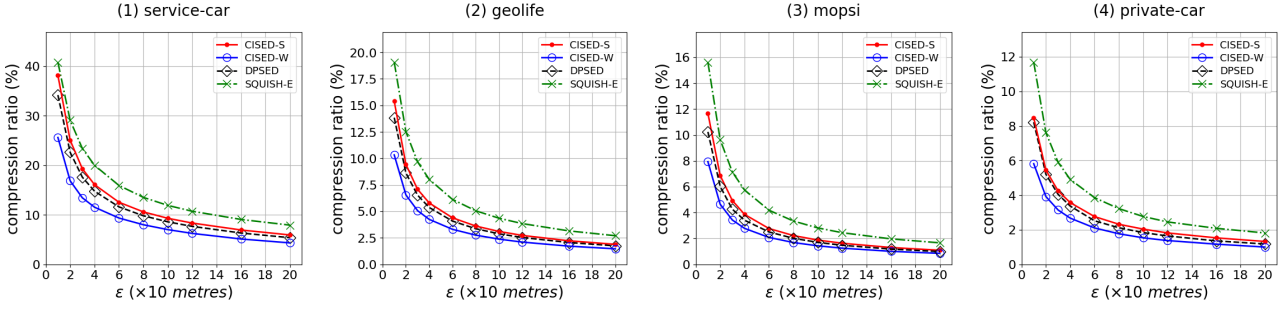


Fig. 13 Evaluation of compression ratios: fixed with $m = 16$ and varying error bound ϵ .

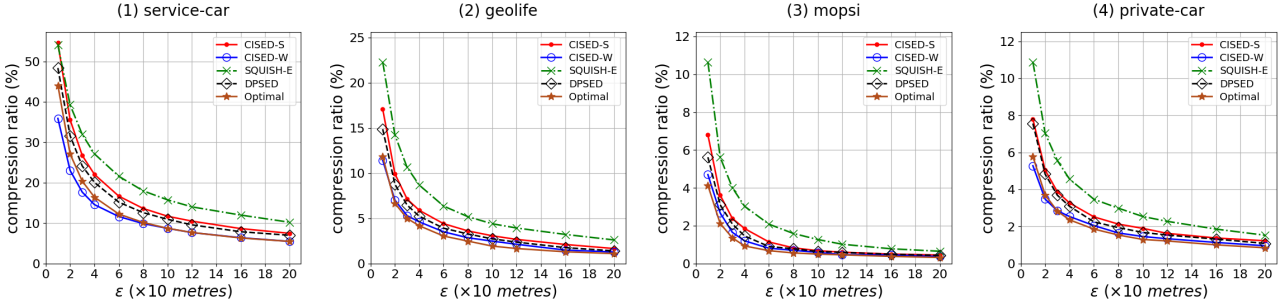


Fig. 14 Evaluation of compression ratios: fixed with $m = 16$ and varying error bound ϵ (on small datasets).

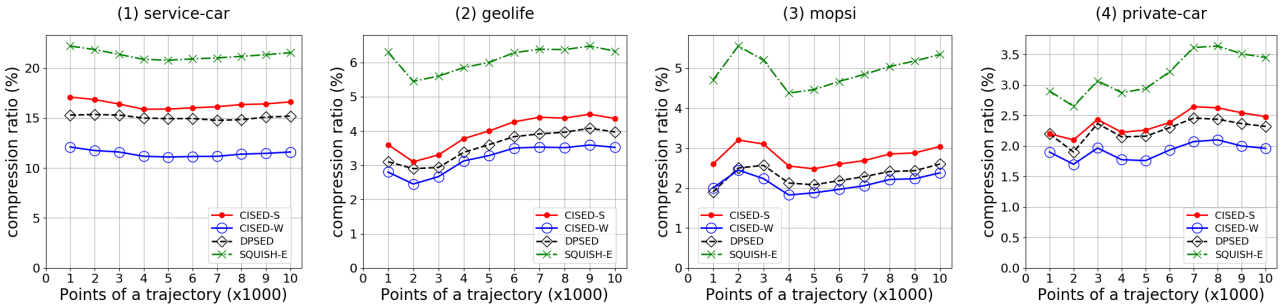


Fig. 15 Evaluation of compression ratios: fixed with $m = 16$ and $\epsilon = 60$ meters, and varying the size of trajectories.

fixed the error bounds $\epsilon = 60$ meters, and varied m from 4 to 40. The results are reported in Figure 12.

(1) Algorithms CISED-S and CISED-W using FastRPolyInter have the same compression ratios as their counterparts using CPolyInter for all cases.

(2) When varying m , the compression ratios of algorithms CISED-S and CISED-W decrease with the increase of m on all datasets.

(3) When varying m , the compression ratios of algorithms CISED-S and CISED-W decrease (a) fast when

$m < 12$, (b) slowly when $m \in [12, 20]$, and (c) very slowly when $m > 20$. Hence, *the region of $[12, 20]$ is the good candidate region for m in terms of compression ratios*. Here the compression ratio of $m=12$ is only on average 100.95% of $m=20$.

Exp-1.2: Impacts of the error bound ϵ on compression ratios (vs. algorithms DPSED and SQUISH-E). To evaluate the impacts of error bound ϵ on compression ratios, we fixed $m=16$, the middle of $[12, 20]$, and varied ϵ from 10 meters to 200 meters on the entire four datasets, respectively. The results are reported in Figure 13 .

(1) When increasing ϵ , the compression ratios of all these algorithms decrease on all datasets.

(2) Dataset PrivateCar has the lowest compression ratios, compared with datasets Mopsi, ServiceCar and GeoLife, due to its highest sampling rate, ServiceCar has the highest compression ratios due to its lowest sampling rate, and GeoLife and Mopsi have the compression ratios in the middle accordingly.

(3) Algorithm CISED-S is better than SQUISH-E and close to DPSED on all datasets and for all ϵ . The compression ratios of CISED-S are on average (79.3%, 71.9%, 67.3%, 72.7%) and (109.2%, 108.0%, 111.7%, 109.1%) of SQUISH-E and DPSED on datasets (ServiceCar, GeoLife, Mopsi, PrivateCar), respectively. For example, when $\epsilon = 40$ meters, the compression ratios of algorithms SQUISH-E, CISED-S and DPSED are (20.0%, 8.0%, 5.7%, 4.9%), (16.1%, 5.8%, 3.9%, 3.6%) and (14.8%, 5.4%, 3.4%, 3.4%) on datasets (ServiceCar, GeoLife, Mopsi, PrivateCar), respectively.

(4) Algorithm CISED-W has better compression ratios than DP, SQUISH-E and CISED-S on all datasets and for all ϵ . The compression ratios of CISED-W are on average (57.7%, 53.8%, 50.0%, 54.6%), (79.5%, 81.0%, 83.0%, 82.0%) and (72.9%, 75.0%, 74.3%, 75.1%) of algorithms SQUISH-E, DPSED and CISED-S on datasets (ServiceCar, GeoLife, Mopsi, PrivateCar), respectively. For example, when $\epsilon = 40$ meters, the compression ratios of algorithm CISED-W are (11.5%, 4.3%, 2.8%, 2.7%) on datasets (ServiceCar, GeoLife, Mopsi, PrivateCar), respectively.

Exp-1.3: Impacts of the error bound ϵ on compression ratios (vs. the optimal algorithm). To evaluate the impacts of error bound ϵ on compression ratios, we again fixed $m=16$, the middle of $[12, 20]$, and varied ϵ from 10 to 200 meters on the first 1K points of each trajectory of the selected *small datasets*, respectively. The results are reported in Figure 14 .

(1) Algorithm CISED-S is worse than the optimal algorithm on all datasets and for all ϵ . More specifically, the compression ratios of CISED-S are on average (134.6%, 150.7%, 155.5%, 138.5%) of the opti-

mal algorithm on datasets (ServiceCar, GeoLife, Mopsi, PrivateCar), respectively. For example, when $\epsilon = 40$ meters, the compression ratios of CISED-S and the optimal algorithm are (22.0%, 5.9%, 1.9%, 3.3%) and (16.4%, 4.2%, 0.9%, 2.4%) on datasets (ServiceCar, GeoLife, Mopsi, PrivateCar), respectively.

(2) Algorithm CISED-W has the closest compression ratios to the optimal algorithm on all datasets and for all ϵ . The compression ratios of CISED-W are on average (94.8%, 115.5%, 119.7%, 107.5%) of the optimal algorithm on datasets (ServiceCar, GeoLife, Mopsi, PrivateCar), respectively. For example, when $\epsilon = 40$ meters, the compression ratios of algorithm CISED-W are (14.6%, 4.6%, 1.2%, 2.5%) on datasets (ServiceCar, GeoLife, Mopsi, PrivateCar), respectively. *This is because algorithm CISED-W allows data interpolations, thus by Proposition 2, it extends the radius of the base circles of the spatio-temporal cones from $\epsilon/2$ in CISED-S to ϵ in CISED-W to include more points.*

Exp-1.4: Impacts of trajectory sizes on compression ratios. To evaluate the impacts of trajectory size, *i.e.*, the number of data points in a trajectory, on compression ratios, we chose the same 10 trajectories from datasets ServiceCar, GeoLife, Mopsi and PrivateCar, respectively, fixed $m=16$ and $\epsilon=60$ meters, and varied the size $|\vec{T}|$ of trajectories from 1K points to 10K points. The results are reported in Figure 15.

(1) The compression ratios of these algorithms ordered from the best to the worst are CISED-W, DPSED, CISED-S and SQUISH-E, on all datasets and for all sizes of trajectories.

(2) The size of input trajectories has few impacts on the compression ratios of LS algorithms on all datasets.

5.2.2 Evaluation of Average Errors

In the second set of tests, we first evaluate the impacts of parameter m on the average errors of algorithms CISED-S and CISED-W, then compare the average errors of our algorithms CISED-S and CISED-W with DPSED, SQUISH-E and the optimal algorithm.

Given a set of trajectories $\{\vec{T}_1, \dots, \vec{T}_M\}$ and their piecewise line representations $\{\vec{T}_1, \dots, \vec{T}_M\}$, and point $P_{j,i}$ denoting a point in trajectory \vec{T}_j contained in a line segment $\mathcal{L}_{l,i} \in \vec{T}_l$ ($l \in [1, M]$), then the average error is $\sum_{j=1}^M \sum_{i=0}^M d(P_{j,i}, \mathcal{L}_{l,i}) / \sum_{j=1}^M |\vec{T}_j|$.

Exp-2.1: Impacts of parameter m on average errors. To evaluate the impacts of parameter m on average errors of algorithms CISED-S and CISED-W, and also to confirm that our fast regular polygon intersection algorithm FastRPolyInter has the same average errors as the convex polygon intersection algorithm CPolyInter, we fixed the error bound $\epsilon = 60$ meters,

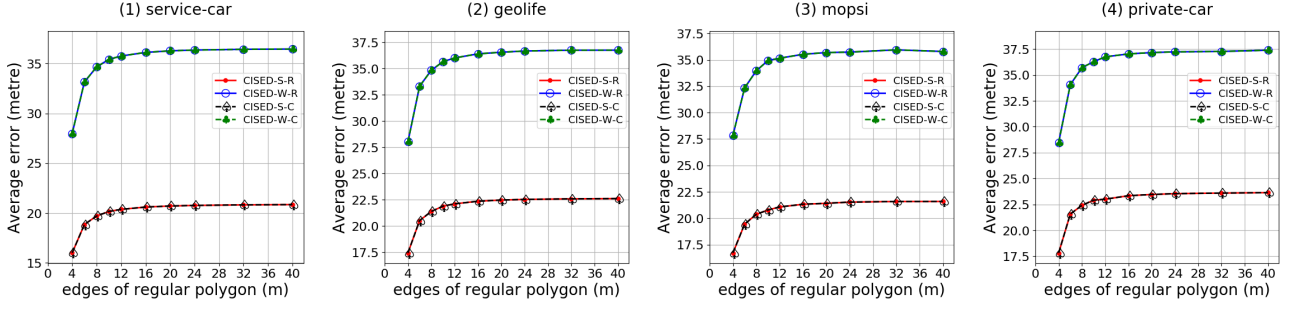


Fig. 16 Evaluation of average errors: fixed error bound with $\epsilon = 60$ meters and varying m . Here “R” denotes our fast regular polygon intersection algorithm FastRPolyInter, and “C” denotes CPolyInter, respectively.

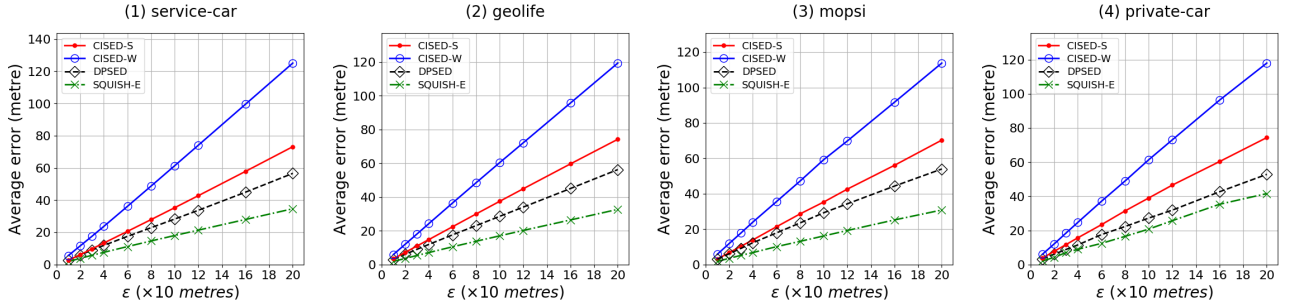


Fig. 17 Evaluation of average errors: fixed with $m = 16$ and varying error bound ϵ .

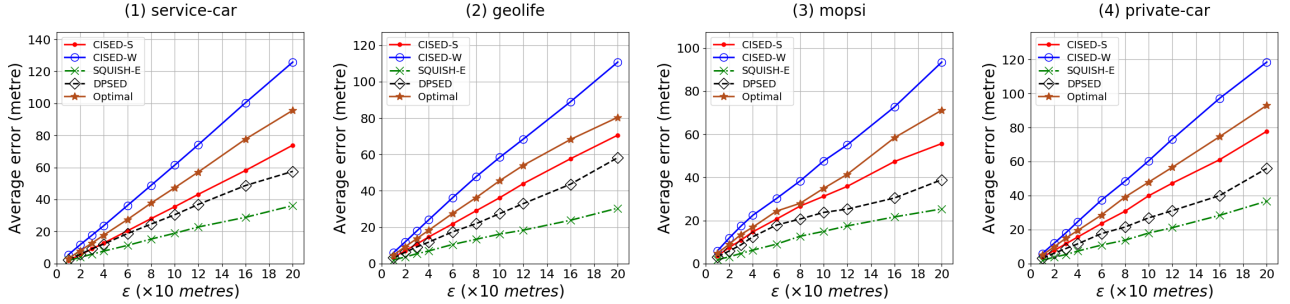


Fig. 18 Evaluation of average errors: fixed with $m = 16$ and varying error bound ϵ (on small datasets).

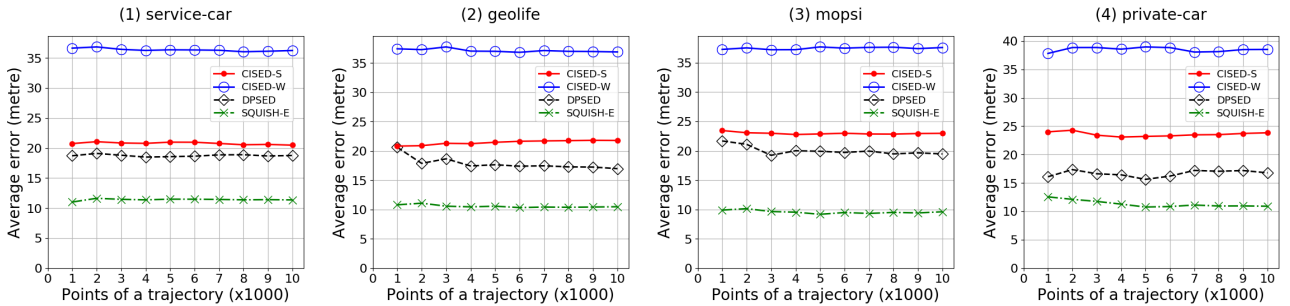


Fig. 19 Evaluation of average errors: fixed with $m = 16$ and $\epsilon = 60$ meters, and varying the size of trajectories.

and varied m from 4 to 40. The results are reported in Figure 16.

(1) Algorithms CISED-S and CISED-W using FastRPolyInter have the same average errors as their counterparts using CPolyInter, respectively, on all datasets and for all m .

(2) When varying m , the average errors of algorithms CISED-S and CISED-W increase with the increase of m on all datasets.

(3) When varying m , similar to compression ratios, the average errors of algorithms CISED-S and CISED-W increase (a) fast when $m < 12$, (b) slowly when

$m \in [12, 20]$, and (c) very slowly when $m > 20$. The range of $[12, 20]$ is also the good candidate region for m in terms of errors. Here the average error of $m = 12$ is only on average 98.49% of $m = 20$.

Exp-2.2: Impacts of the error bound ϵ on average errors (vs. algorithms DPSED and SQUISH-E). To evaluate the average errors of these algorithms, we fixed $m=16$, and varied ϵ from 10 to 200 meters on the entire datasets ServiceCar, GeoLife, Mopsi and PrivateCar, respectively. The results are reported in Figure 17.

- (1) Average errors increase with the increase of ϵ .
- (2) The average errors of these algorithms from the largest to the smallest are CISED-W, CISED-S, DPSED and SQUISH-E, on all datasets and for all ϵ . The average errors of algorithms CISED-S and CISED-W are on average (119.3%, 127.7%, 119.9%, 138.0%) and (210.1%, 207.5%, 200.9%, 217.5%) of DPSED and (188.2%, 215.2%, 212.8%, 180.3%) and (331.1%, 349.7%, 356.7%, 284.2%) of SQUISH-E on datasets (ServiceCar, GeoLife, Mopsi, PrivateCar), respectively.
- (3) When the error bound of algorithm CISED-W is set as the half of CISED-S, the average errors of CISED-W are on average (93.8%, 86.0%, 81.4%, 79.4%) of CISED-S on datasets (ServiceCar, GeoLife, Mopsi, PrivateCar), respectively, meaning that the large average errors of algorithm CISED-W are caused by its cone *w.r.t.* ϵ compared with the narrow cone *w.r.t.* $\epsilon/2$ of CISED-S.

Exp-2.3: Impacts of the error bound ϵ on average errors (vs. the optimal algorithm). To evaluate the average errors of these algorithms, we fixed $m=16$, and varied ϵ from 10 to 200 meters on the first 1K points of each trajectory of the selected *small datasets*, respectively. The results are reported in Figure 18.

The average errors of these algorithms from the largest to the smallest are CISED-W, the optimal algorithm and CISED-S, on all datasets and for all ϵ . The average errors of CISED-S and CISED-W are on average (73.6%, 80.7%, 85.1%, 81.0%) and (133.3%, 130.7%, 131.0%, 126.3%) of the optimal algorithm on datasets (ServiceCar, GeoLife, Mopsi, PrivateCar), respectively.

Exp-2.4: Impacts of trajectory sizes on average errors. To evaluate the impacts of trajectory sizes on average errors, we chose the same 10 trajectories from datasets ServiceCar, GeoLife, Mopsi and PrivateCar, respectively. We fixed $m=16$ and $\epsilon = 60$ meters, and varied the size $|\vec{T}|$ of trajectories from 1K points to 10K points. The results are reported in Figure 19.

- (1) The average errors of these algorithms ordered from the smallest to the largest are SQUISH-E, DPSED, CISED-S and CISED-W, on all datasets and for all trajectory sizes.

- (2) The size of input trajectories has few impacts on the average errors of LS algorithms on all datasets.

5.2.3 Evaluation of Running Time

In the third set of tests, we evaluate the impacts of parameter m on the running time of algorithms CISED-S and CISED-W, and compare the running time of our approaches CISED-S and CISED-W with the optimal algorithm and algorithms DPSED and SQUISH-E.

Exp-3.1: Impacts of algorithm FastRPolyInter and parameter m on running time. To evaluate the impacts of parameter m on the running time of algorithm CISED-S and CISED-W, and also to confirm that our fast regular polygon intersection algorithm FastRPolyInter runs faster than the convex polygon intersection algorithm CPolyInter, we equipped CISED-S and CISED-W with FastRPolyInter and CPolyInter, respectively, fixed $\epsilon = 60$ meters, and varied m from 4 to 40. The results are reported in Figures 20 and 21.

- (1) The algorithms CISED-S and CISED-W spend the most time in the execution of polygon intersections. For all m , the execution time of algorithms CPolyInter and FastRPolyInter is on average (93.5%, 96.0%, 94.5%, 92.0%) and (90.5%, 92.5%, 91.0%, 90.5%) of the entire compression time on datasets (ServiceCar, GeoLife, Mopsi, PrivateCar), respectively.
- (2) FastRPolyInter runs faster than CPolyInter on all datasets and for all m . The execution time of algorithms CISED-S-FastRPolyInter and CISED-W-FastRPolyInter is one average 83.74% their counterparts with CPolyInter.
- (3) When varying m , the execution time of algorithms CISED-S-FastRPolyInter, CISED-S-CPolyInter, CISED-W-FastRPolyInter and CISED-W-CPolyInter increases approximately linearly with the increase of m on all the datasets.
- (4) The running time of $m = 12$ is on average 69.92% of $m = 20$ for CISED-S and CISED-W on all datasets.

Exp-3.2: Impacts of the error bound ϵ on running time (VS. algorithms DPSED and SQUISH-E). To evaluate the impacts of ϵ on running time, we fixed $m = 16$, and varied ϵ from 10 meters to 200 meters on the entire datasets (ServiceCar, GeoLife, Mopsi, PrivateCar), respectively. The results are reported in Figure 22.

- (1) All algorithms are not very sensitive to ϵ on any datasets, and algorithm DPSED is more sensitive to ϵ than the other three algorithms. The running time of DPSED decreases a little bit with the increase of ϵ , as the increment of ϵ decreases the number of partitions of the input trajectory.
- (2) Algorithms CISED-S and CISED-W are obviously faster than DPSED and SQUISH-E for all cases. They

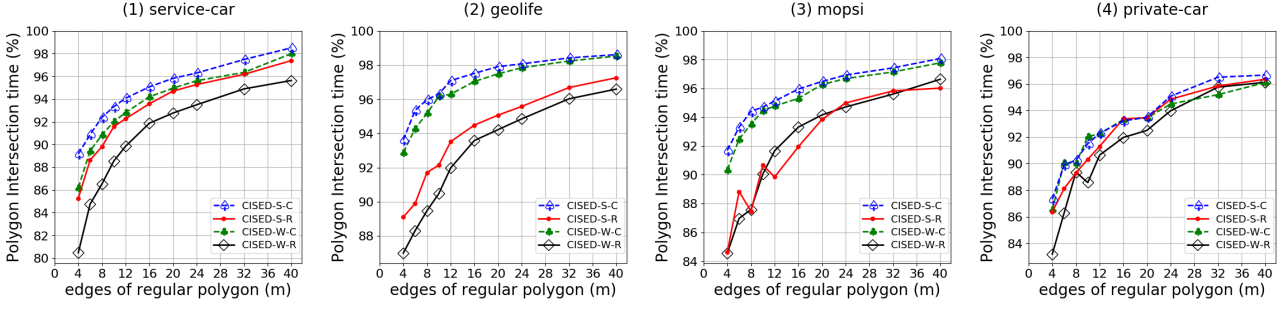


Fig. 20 Evaluation of running time of polygon intersection algorithms: fixed error bound with $\epsilon = 60$ meters, and varying m . Here “R” denotes our fast regular polygon intersection algorithm FastRPolyInter, and “C” denotes CPolyInter, respectively.

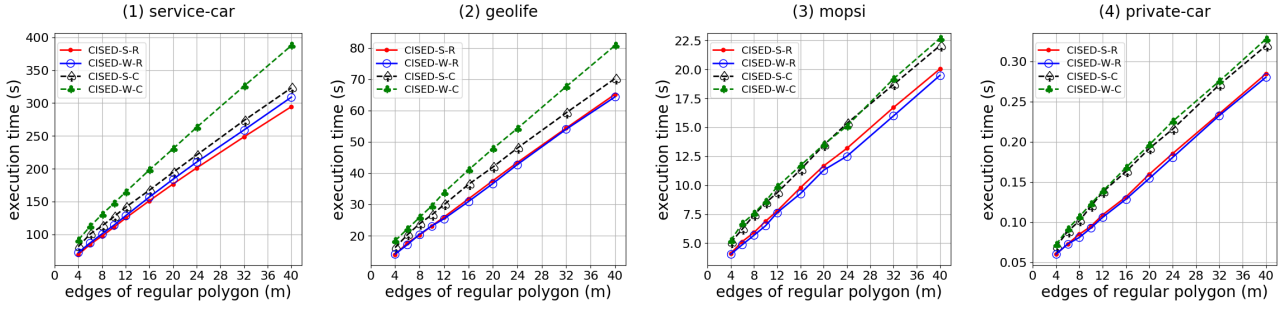


Fig. 21 Evaluation of running time: fixed error bound with $\epsilon = 60$ meters, and varying m .

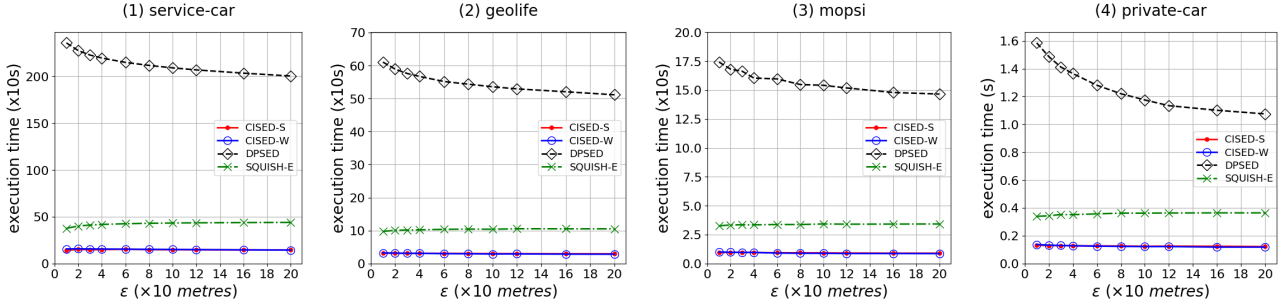


Fig. 22 Evaluation of running time: fixed with $m = 16$ and varying error bounds ϵ .

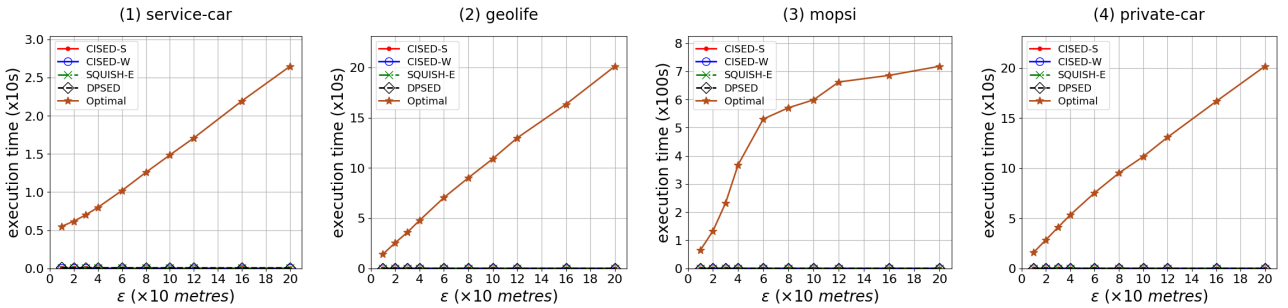


Fig. 23 Evaluation of running time: fixed with $m = 16$ and varying error bounds ϵ (on small datasets).

are on average (14.21, 18.19, 17.06, 9.98) times faster than DPSED, and (2.84, 3.45, 3.69, 2.86) times faster than SQUISH-E on datasets (ServiceCar, GeoLife, Mopsi, PrivateCar), respectively.

Exp-3.3: Impacts of the error bound ϵ on running time (VS. the optimal algorithm). To eval-

uate the impacts of ϵ on running time, we fixed $m = 16$, and varied ϵ from 10 to 200 meters on the first 1K points of each trajectory of the selected *small datasets*, respectively. The results are reported in Figure 23.

(1) Algorithms CISED-S and CISED-W are obviously faster than the optimal algorithm for all cases. They

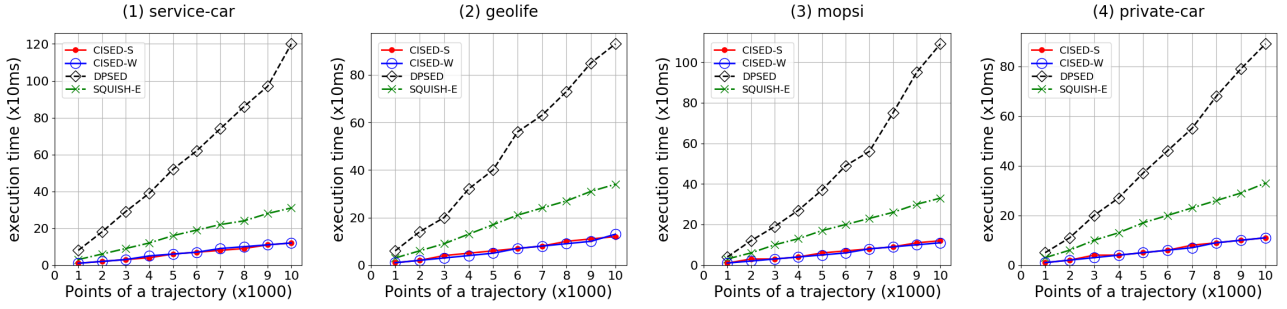


Fig. 24 Evaluation of running time: fixed with $m = 16$ and $\epsilon = 60$ meters, and varying the size of trajectories.

are on average (925.25, 7888.26, 40041.59, 8528.76) times faster than the optimal algorithm on datasets (ServiceCar, GeoLife, Mopsi, PrivateCar), respectively.

Exp-3.4: Impacts of trajectory sizes on running time. To evaluate the impacts of trajectory sizes on running time, we chose the same 10 trajectories, from datasets (ServiceCar, GeoLife, Mopsi, PrivateCar), respectively, fixed $m = 16$ and $\epsilon = 60$ meters, and varied the size $|\vec{T}|$ of trajectories from 1K points to 10K points. The results are reported in Figure 24.

(1) Algorithms CISED-S and CISED-W are both the fastest LS algorithms using SED, and are (8.00–10.00, 5.83–8.11, 4.00–9.50, 5.00–8.09) times faster than DPSED, and (2.53–3.00, 2.62–3.12, 2.50–3.33, 2.89–3.40) times faster than SQUISH-E on the selected 1K to 10K points datasets (ServiceCar, GeoLife, Mopsi, PrivateCar), respectively.

(2) Algorithms CISED-S and CISED-W scale well with the increase of the size of trajectories on all datasets, and both have a linear running time, while algorithm DPSED does not. This is consistent with their time complexity analyses.

(3) The advantage of running time of algorithms CISED-S and CISED-W increases with the increase of trajectory sizes compared with DPSED and SQUISH-E.

5.2.4 Evaluation of Distance Metrics PED vs. SED

In the last set of tests, we compare the performance of algorithms using PED vs. SED. Two pairs of algorithms are tested, namely, (1) the algorithm DP using PED and SED, respectively, and (2) the sector intersection algorithm [36, 40] using PED and our spatio-temporal cone intersection algorithm using SED.

Exp-4.1: Impacts of distance metrics on compression ratios. To evaluate the impacts of distance metrics, *i.e.*, PED and SED, on compression ratios, we fixed $m=16$ and varied ϵ from 10 meters to 200 meters on the entire four datasets, respectively. The results are reported in Figure 25.

Given the same error bound ϵ , the compression ratios using PED are obviously better than using SED. More specifically, the compression ratios of algorithms DP using PED are on average (47.1%, 55.5%, 60.7%, 44.7%) of algorithm DP using SED and the compression ratio of algorithm CISED-S is on average (45.4%, 54.5%, 60.1%, 43.0%) of algorithm SQUISH-E on datasets (ServiceCar, GeoLife, Mopsi, PrivateCar), respectively.

Exp-4.2: Impacts of distance metrics on average errors. To evaluate the impacts of distance metrics on average errors, we fixed $m=16$ and varied ϵ from 10 to 200 meters on the entire four datasets, respectively. The results are reported in Figure 26.

Given the same error bound ϵ , the average errors of algorithms using SED are a bit larger than using PED. The average errors of DP using PED is on average (76.7%, 77.6%, 79.7%, 63.0%) of DP using SED, and the average errors of algorithm SQUISH-E is on average (97.5%, 78.1%, 92.4%, 74.2%) of algorithm CISED-S on datasets (ServiceCar, GeoLife, Mopsi, PrivateCar), respectively.

Exp-4.3: Impacts of distance metrics on running time. To evaluate the impacts of distance metrics on running time, we also fixed $m=16$ and varied ϵ from 10 to 200 meters on the entire four datasets, respectively. The results are reported in Figure 27.

Given the same error bound ϵ , the running time of DP using PED is on average (24.3%, 119.9%, 23.4%, 91.3%) of DP using SED, and the running time of algorithm SQUISH-E is on average (7.0%, 36.3%, 19.9%, 69.2%) of algorithm CISED-S on datasets (ServiceCar, GeoLife, Mopsi, PrivateCar), respectively.

5.2.5 Summary and Discussion

Summary. From these tests we find the following:

(1) *Datasets.* The behaviors of all algorithms across all datasets are quite similar.

(2) *Polygon intersection Algorithms.* Algorithm FastRPolyInter runs faster than algorithm CPolyInter, and has the same compression ratios and average errors as CPolyInter.

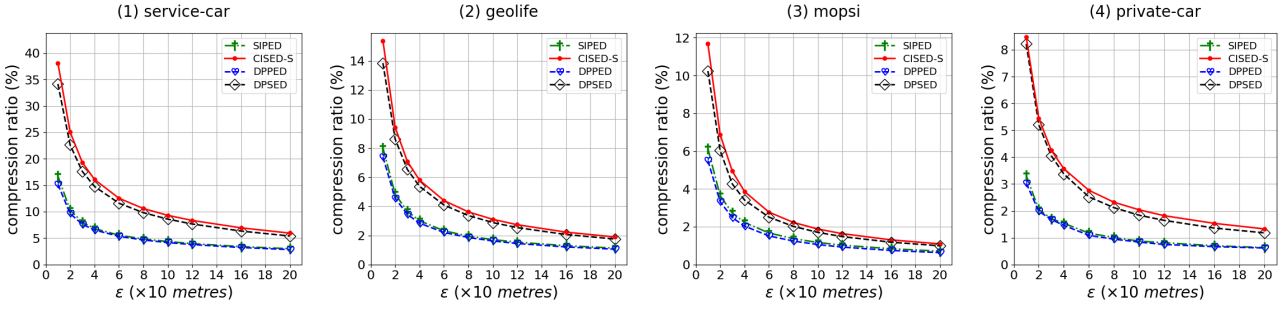


Fig. 25 Evaluation of compression ratios (PED vs. SED): fixed with $m = 16$ and varying error bound ϵ .

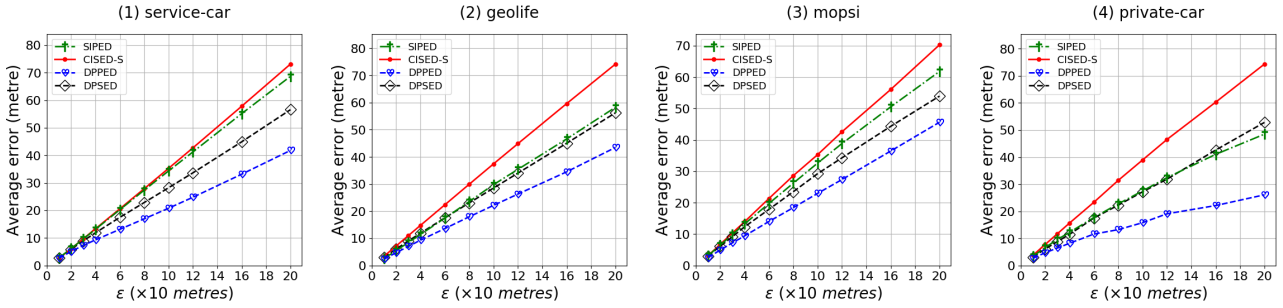


Fig. 26 Evaluation of average errors (PED vs. SED): fixed with $m = 16$ and varying error bound ϵ .

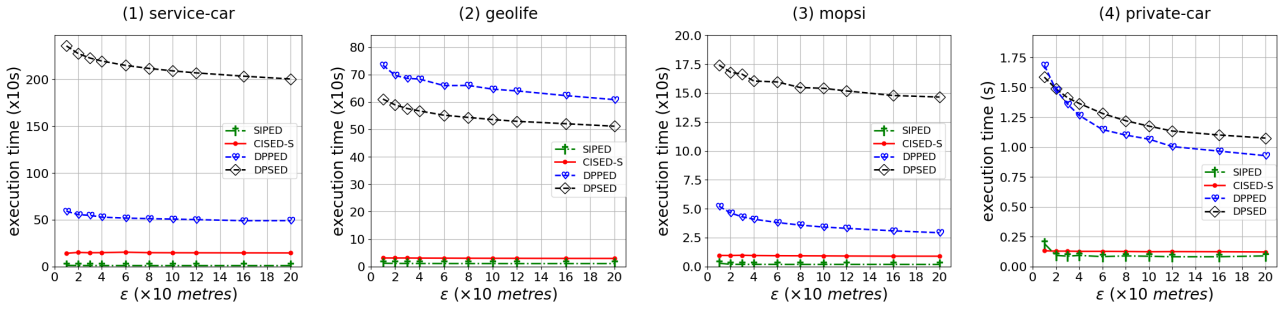


Fig. 27 Evaluation of running time (PED vs. SED): fixed with $m = 16$ and varying error bounds ϵ .

(3) *Parameter m .* The compression ratio decreases with the increase of m , and the running time increases nearly linearly with the increase of m . In practice, the range of $[12, 20]$ is a good candidate region for m .

(4) *Compression ratios.* The optimal LS algorithm has the best compression ratios among all strong simplification algorithms. Algorithm CISED-S is close to DPSED and algorithm CISED-W is better than all the sub-optimal LS algorithm. The compression ratios of algorithm CISED-S, the optimal algorithm and algorithm CISED-W are on average (79.3%, 71.9%, 67.3%, 72.7%), (58.1%, 45.1%, 39.2%, 52.8%) and (57.7%, 53.8%, 50.0%, 54.6%) of SQUISH-E and (109.2%, 108.0%, 111.7%, 109.1%), (81.3%, 75.5%, 72.5%, 78.1%) and (79.5%, 81.0%, 83.0%, 82.0%) of DPSED on datasets (ServiceCar, GeoLife, Mopsi, PrivateCar), respectively.


(5) *Average errors.* The average errors of these algorithms from the smallest to the largest are SQUISH-

E, DPSED, CISED-S, the optimal LS algorithm and CISED-W. Algorithm CISED-W has obvious higher average errors than CISED-S as the former essentially forms spatio-temporal cones with a radius of ϵ .

(6) *Running time.* Algorithms CISED-S and CISED-W are the fastest. They are on average (14.21, 18.19, 17.06, 9.98), (2.84, 3.45, 3.69, 2.86) and (925.25, 7888.26, 40041.59, 8528.76) times faster than DPSED, SQUISH-E and the optimal LS algorithm on datasets (ServiceCar, GeoLife, Mopsi, PrivateCar), respectively. The advantage of running time of algorithms CISED-S and CISED-W also increases with the increase of the trajectory size.

(7) *Distance metrics.* Compared with PED, SED supports spatio-temporal queries. However, it comes a price, e.g., the compression ratios of algorithms using PED are better than those using SED.

Discussion. We next briefly discuss the choice of algorithms to compress trajectories. As different applica-


tions  have different requirements to reach a balance among multiple metrics, we only provide a brief guideline from the views of running time, compression ratio and average error, respectively.

(1) When the running time is the first-level consideration or algorithms are run in resource-constrained devices, then the one-pass algorithms, *i.e.*, CISED-S and CISED-W, are surely the best choices, and they have pretty good compression ratios at the same time.

(2) When the compression ratio is the priority, then algorithm CISED-W and the optimal algorithm are the selections, followed by algorithms DPSED and CISED-S.


(3) When considering error, SQUISH-E is a good choice because it has a relative small average error. Alternatively, we can also use DPSED or CISED-S by setting a smaller error bound ϵ compared with SQUISH-E.

6 Related Work

Trajectory compression algorithms are normally classified into two categories, namely lossless compression and lossy compression [23]. (1) Lossless compression methods enable exact reconstruction of the original data from the compressed data without information loss. (2) In contrast, *lossy* compression methods allow errors or *derivation*  compared with the original trajectories. These techniques typically identify important data points, and remove statistical redundant data points from a trajectory, or replace original data points in a trajectory with other places of interests, such as roads and shops. They focus on good compression ratios with acceptable errors. In this work, we focus on lossy compression of trajectory data, and we next introduce the related work on lossy trajectory compression from two aspects: line simplification based methods and semantics based methods.

6.1 Line simplification based methods

The idea of piece-wise line simplification comes from computational geometry. Its target is to approximate a given finer piece-wise linear curve by another coarser piece-wise linear curve, which is typically a subset of the former, such that the maximum distance of the former to the later is bounded by a user specified bound ϵ . Initially, line simplification (LS) algorithms use perpendicular Euclidean distances (PED) as the distance metric. Then a new distance metric, the synchronous Euclidean distances (SED), was developed after the LS algorithms were introduced to compress trajectories. SED was first introduced in the name of *time-ratio distance* in [20],

and formally presented in [29] as the *synchronous Euclidean distance*. PED and SED are two common metrics adopted in trajectory simplification. The former usually brings better compression ratios while the later reserves temporal information in the result trajectories. 

Line simplification algorithms can be classified into two aspects: optimal and sub-optimal methods.

6.1.1 Optimal Algorithms

For the “min-#” problem that finds out the minimal number of points or segments to represent the original polygonal lines *w.r.t.* an error bound ϵ , Imai and Iri [14] first formulated it as a graph problem, and showed that it could be solved in $O(n^3)$ time, where n is the number of the original points. Toussaint of [38] and Melkman and O’Rourke of [19] improved the time complexity to $O(n^2 \log n)$ by using either *convex hull* or *sector intersection* methods. The authors of [3] further proved that the optimal algorithm using PED could be implemented in $O(n^2)$ time by using the *sector intersection* mechanism. Because the *sector intersection* and the *convex hull* mechanisms can not work with SED, hence, currently the time complexity of the optimal algorithm using SED remains $O(n^3)$. It is time-consuming and impractical for large trajectory data [11].





6.1.2 Sub-optimal Algorithms

Many studies have been targeting at finding the sub-optimal results. In particular, the state-of-the-art of sub-optimal LS approaches fall into three categories, *i.e.*, batch, online and one-pass algorithms. We next introduce these LS based trajectory compression algorithms from the aspect of the three categories.

Batch algorithms. The batch algorithms adopt a global distance checking policy that requires all trajectory points are loaded before compressing starts. These batch algorithms can be either top-down or bottom-up.

Top-down algorithms, *e.g.*, Ramer [30] and Douglas-Peucker [7], recursively divide a trajectory into sub-trajectories until the stopping condition is met. Bottom-up algorithms, *e.g.*, Theo Pavlidis’ algorithm [26], is the natural complement of the top-down ones, which recursively merge adjacent sub-trajectories with the smallest distance, initially $n/2$ sub-trajectories for a trajectory with n points, until the stopping condition is met. The distances of newly generated line segments are recalculated during the process. These batch algorithms originally only support PED, but are easy to be extended to support SED [20]. The batch nature and high time complexities make batch algorithms impractical for online and resource-constrained scenarios [15].

Online algorithms. The online algorithms adopt a constrained global distance checking policy that restricts the checking within a sliding or opening window. Constrained global checking algorithms do not need to have the entire trajectory ready before they start compressing, and are more appropriate than batch algorithm for compressing trajectories for online scenarios.



Several LS algorithms have been developed, e.g., by combining DP or Theo Pavlidis' with sliding or opening windows for online processing [20]. These methods still have a high time and/or space complexity, which significantly hinders their utility in resource-constrained mobile devices [16]. BQS [16,17] and SQUISH-E [23] further optimize the opening window algorithms. BQS [16,17] asts the processing by picking out at most eight special points from an open window based on a convex hull, which, however, hardly supports SED. The SQUISH-E [23] algorithm is an  combination of opening window and bottom-up  online algorithm t uses a doubly linked list Q to achieve a better efficiency. Although SQUISH-E supports SED, it is not one-pass, and has a relatively poor compression ratio.

One-pass algorithms. The one-pass algorithms adopt a local distance checking policy. They do not need a window to buffer the previously read points as they process each point in a trajectory once and only once. Obviously, the one-pass algorithms run in linear time and constant space.

The n -th point routine and the routine of random-selection of points [35] are two naive one-pass algorithms. In these routines, for every fixed number of consecutive points along the line, the n -th point and one random point among them are retained, respectively. They are fast, but are obviously not error bounded. In Reumann-Witkam routine [31], it builds a strip paralleling to the line connecting the first two points, then the points within this strip compose one section of the line. The Reumann-Witkam routine also runs fast, but has limited compression ratios. The sector intersection (SI) algorithm [36,40] was developed for graphic and pattern recognition in the late 1970s, for the approximation of arbitrary planar curves by linear segments or finding a polygonal approximation of a set of input data points in a 2D Cartesian coordinate system. [8] optimized algorithm SI by considering the distance between a potential end point and the initial point of a line segment, and the Sleeve algorithm [42] in the cartographic discipline essentially applies the same idea as the SI algorithm. Moreover, fast BQS [16] (FBQS in short), the simplified version of BQS, has a linear time complexity. The authors of this article also developed a One-Pass Error Bounded (OPERB) algorithm [15]. However, all existing

one-pass algorithms use PED [8,15,16,36,40,42], while this study focuses on SED.

6.2 Semantics based methods

The trajectories of certain moving objects such as cars and trucks are constrained by road networks. These moving objects typically travel along road networks, instead of the line segment between two points. Trajectory compression methods based on road networks [5,6,9,10,13,28,37] project trajectory points onto roads (also known as Map-Matching). Moreover, [9,10,37] mine and use high frequency patterns of compressed trajectories, instead of roads, to further improve compression effectiveness. Some methods [32,33] compress trajectories beyond the use of road networks, and further make use of other user specified domain knowledge, such as places of interests along the trajectories [32].  There are also compression algorithms preserving the direction of the trajectory [18]. 

These semantics based approaches are orthogonal to line simplification based methods, and may be combined with each other to improve the effectiveness of trajectory compression.

7 Conclusions

We have proposed CISED-S and CISED-W, two one-pass error bounded strong and weak trajectory simplification algorithms using the synchronous distance. We have also experimentally verified that algorithms CISED-S and CISED-W are fast and have good compression ratios. They are three times faster than SQUISH-E, the fastest existing LS algorithm using SED. In terms of compression ratio, algorithm CISED-S is close to DPSED, the existing LS algorithm with the best compression ratio, and is 21.1% better than SQUISH-E on average; and algorithm CISED-W is better than all the sub-optimal algorithm and is on average 19.6% and 42.4% better than DPSED and SQUISH-E, respectively.

Acknowledgments

This work is supported in part by NSFC (U1636210) and 973 program (2014CB340300).

Appendix: Proofs

Proof of Proposition 1: Let P'_{s+i} ($i \in [1, k]$) be the intersection point of line segment $\overrightarrow{P_s Q}$ and the plane $P.t - P_{s+i}.t = 0$. It suffices to show that the intersection

point P'_{s+i} satisfies that (1) $P'_{s+i}.t = P_{s+i}.t$, (2) $P'_{s+i}.x = P_s.x + w \cdot (Q.x - P_s.x)$, and (3) $P'_{s+i}.y = P_s.y + w \cdot (Q.y - P_s.y)$, where $w = \frac{P'_{s+i}.t - P_s.t}{Q.t - P_s.t} = \frac{P_{s+i}.t - P_s.t}{Q.t - P_s.t}$. Hence, P'_{s+i} is indeed a synchronized point of P_{s+i} w.r.t. $\overrightarrow{P_s Q}$, and the distance $|P_{s+i} P'_{s+i}|$ from P_{s+i} to P'_{s+i} is the synchronous distance of P_{s+i} to $\overrightarrow{P_s Q}$.

We assume first that $\bigcap_{i=1}^k \mathcal{C}(P_s, \mathcal{O}(P_{s+i}, \epsilon)) \neq \{P_s\}$. Then there must exist a point Q in the area of the synchronous circle $\mathcal{O}(P_{s+k}, \epsilon)$ such that $\overrightarrow{P_s Q}$ passes through all the cones $\mathcal{C}(P_s, \mathcal{O}(P_{s+i}, \epsilon))$ $i \in [1, k]$. Hence, $Q.t = P_{s+k}.t$. We also have $sed(P_{s+i}, \overrightarrow{P_s Q}) = |P'_{s+i} P_{s+i}| \leq \epsilon$ for each $i \in [1, k]$ since P'_{s+i} is in the area of circle $\mathcal{O}(P_{s+i}, \epsilon)$.

Conversely, assume that there exists a point Q such that $Q.t = P_{s+k}.t$ and $sed(P_{s+i}, \overrightarrow{P_s Q}) \leq \epsilon$ for all P_{s+i} ($i \in [1, k]$). Then $|P'_{s+i} P_{s+i}| \leq \epsilon$ for all $i \in [1, k]$. Hence, we have $\bigcap_{i=1}^k \mathcal{C}(P_s, \mathcal{O}(P_{s+i}, \epsilon)) \neq \{P_s\}$. \square

Proof of Proposition 2: By Proposition 1, it suffices to show that $\bigcap_{i=1}^k \mathcal{O}^c(P_{s+i}^c, r_{s+i}^c) \neq \emptyset$ if and only if $\bigcap_{i=1}^k \mathcal{C}(P_s, \mathcal{O}(P_{s+i}, \epsilon)) \neq \{P_s\}$, which is obvious. Hence, we have the conclusion. \square

Proof of Proposition 3: We shall prove this by contradiction. Assume first that $\mathcal{R}_l^* \cap \mathcal{R}_{s+l+1}$ has more than m edges. Then it must have two distinct edges $\overrightarrow{A_i}$ and $\overrightarrow{A_{i'}}$ with the same label j ($1 \leq j \leq m$), originally from \mathcal{R}_{s+i} and $\mathcal{R}_{s+i'}$ ($1 \leq i < i' \leq l+1$). Note that here $\mathcal{R}_{s+i} \cap \mathcal{R}_{s+i'} \neq \emptyset$ since $\mathcal{R}_l^* \cap \mathcal{R}_{s+l+1} \neq \emptyset$. However, when $\mathcal{R}_{s+i} \cap \mathcal{R}_{s+i'} \neq \emptyset$, the intersection $\mathcal{R}_{s+i} \cap \mathcal{R}_{s+i'}$ cannot have both edge $\overrightarrow{A_i}$ and edge $\overrightarrow{A_{i'}}$, as all edges with the same label are in parallel (or overlapping) with each other by the above definition of inscribed regular polygons. This contradicts with the assumption. \square

Proof of Proposition 4: The inscribed regular polygon \mathcal{R}_{s+l+1} has m edges, and intersection polygon \mathcal{R}_l^* has at most m edges by Proposition 3. As the intersection of two m -edges convex polygons can be computed in $O(m)$ time [25], the intersection of polygons \mathcal{R}_l^* and \mathcal{R}_{s+l+1} can be done in $O(1)$ time for a fixed m . \square

Proof of Proposition 5: If $(\vec{A} \cap \vec{B} \neq \emptyset \text{ and } \vec{A} \times \vec{B} < 0 \text{ and } P_{e_A} \notin \mathcal{H}(\vec{B}))$ or $(\vec{A} \cap \vec{B} \neq \emptyset \text{ and } \vec{A} \times \vec{B} \geq 0 \text{ and } P_{e_B} \in \mathcal{H}(\vec{A}))$, then as all edges in the same edge groups E^j ($1 \leq j \leq m$) are in parallel with each other and by the geometric properties of regular polygon \mathcal{R}_{s+k+1} , it is easy to find that, for each position of \vec{A} between its original to its opposite positions, we have (1) $\vec{A} \cap \vec{B} = \emptyset$, and (2) either $P_{e_A} \notin \mathcal{H}(\vec{B})$ or $P_{e_B} \in \mathcal{H}(\vec{A})$. Hence, by the advance rule (1) of algorithm CPolyInter in Section 2.4, edge \vec{A} is always moved forward until it reaches the opposite position of its original one. From this, we have the conclusion. \square

Proof of Proposition 6: If $(\vec{A} \cap \vec{B} \neq \emptyset \text{ and } \vec{A} \times \vec{B} \geq 0 \text{ and } P_{e_B} \notin \mathcal{H}(\vec{A}))$ or $(\vec{A} \cap \vec{B} \neq \emptyset \text{ and } \vec{A} \times \vec{B} < 0 \text{ and } P_{e_A} \in \mathcal{H}(\vec{B}))$, then it is also easy to find that, for each position of \vec{B} between its original to its target positions (i.e., the edge after the one having the same edge group as \vec{A}), we have (1) $\vec{A} \cap \vec{B} = \emptyset$, and (2) either $P_{e_B} \notin \mathcal{H}(\vec{A})$ or $P_{e_A} \in \mathcal{H}(\vec{B})$. Hence, by the advance rule (2) of algorithm CPolyInter in Section 2.4, edge \vec{B} is always moved forward until it reaches the target position. From this, we have the conclusion. \square

Proof of Proposition 8: If $\bigcap_{i=s+1}^e \mathcal{C}(P_s, P_{s+i}, \epsilon/2) \neq \{P_s\}$, then by Proposition 1, there exists a point Q , $Q.t = P_{s+k}.t$, such that $sed(P_{s+i}, \overrightarrow{P_s Q}) \leq \epsilon/2$ for all $i \in [1, k]$. By the triangle inequality essentially, $sed(P_{s+i}, \overrightarrow{P_s P_{s+k}}) \leq sed(P_{s+i}, \overrightarrow{P_s Q}) + |Q P_{s+k}| \leq \epsilon/2 + \epsilon/2 = \epsilon$. \square

Proof of Proposition 9: By Proposition 2 and the nature of inscribed regular polygon, it is easy to find that for any point $Q \in \mathcal{R}_k^*$ w.r.t. plane $t_c = P_{s+k}.t$, there is $sed(P_{s+i}, \overrightarrow{P_s Q}) \leq \epsilon$ for all points P_{s+i} ($i \in [1, k]$). From this, we have the conclusion. \square

References

1. Mopsi routes 2014. <http://cs.uef.fi/mopsi/routes/dataset/>. Accessed: 2017-11-29.
2. H. Cao, O. Wolfson, and G. Trajcevski. Spatio-temporal data reduction with deterministic error bounds. *VLDBJ*, 15(3):211–228, 2006.
3. W. Chan and F. Chin. Approximation of polygonal curves with minimum number of line segments or minimal error. *International Journal of Computational Geometry Applications*, 6(1):378–387, 1996.
4. M. Chen, M. Xu, and P. Fränti. A fast multiresolution polygonal approximation algorithm for GPS trajectory simplification. *IEEE Trans. Image Processing*, 21(5):2770–2785, 2012.
5. Y. Chen, K. Jiang, Y. Zheng, C. Li, and N. Yu. Trajectory simplification method for location-based social networking services. In *LBSN*, pages 33–40, 2009.
6. A. Civilis, C. S. Jensen, and S. Pakalnis. Techniques for efficient road-network-based tracking of moving objects. *TKDE*, 17(5):698–712, 2005.
7. D. H. Douglas and T. K. Peucker. Algorithms for the reduction of the number of points required to represent a digitized line or its caricature. *The Canadian Cartographer*, 10(2):112–122, 1973.
8. J. G. Dunham. Piecewise linear approximation of planar curves. *PAMI*, 8, 1986.
9. R. Gotsman and Y. Kanza. A dilation-matching-encoding compaction of trajectories over road networks. *GeoInformatica*, 2015.
10. Y. Han, W. Sun, and B. Zheng. Compress: A comprehensive framework of trajectory compression in road networks. *TODS*, 42(2):11:1–11:49, 2017.
11. P. S. Heckbert and M. Garland. Survey of polygonal surface simplification algorithms. In *SIGGRAPH*, 1997.
12. J. Hershberger and J. Snoeyink. Speeding up the douglas-peucker line-simplification algorithm. *Technical Report, University of British Columbia*, 1992.

13. C. C. Hung, W. Peng, and W. Lee. Clustering and aggregating clues of trajectories for mining trajectory patterns and routes. *VLDBJ*, 24(2):169–192, 2015.
14. H. Imai and M. Iri. Computational-geometric methods for polygonal approximations of a curve. *Computer Vision Graphics and Image Processing*, 36:31–41, 1986.
15. X. Lin, S. Ma, H. Zhang, T. Wo, and J. Huai. One-pass error bounded trajectory simplification. *PVLDB*, 10(7):841–852, 2017.
16. J. Liu, K. Zhao, P. Sommer, S. Shang, B. Kusy, and R. Jurdak. Bounded quadrant system: Error-bounded trajectory compression on the go. In *ICDE*, 2015.
17. J. Liu, K. Zhao, P. Sommer, S. Shang, B. Kusy, J.-G. Lee, and R. Jurdak. A novel framework for online amnesic trajectory compression in resource-constrained environments. *IEEE Transactions on Knowledge and Data Engineering*, 28(11):2827–2841, 2016.
18. C. Long, R. C.-W. Wong, and H. Jagadish. Direction-preserving trajectory simplification. *PVLDB*, 6(10):949–960, 2013.
19. A. Melkman and J. O’Rourke. On polygonal chain approximation. *Machine Intelligence and Pattern Recognition*, 6:87–95, 1988.
20. N. Meratnia and R. A. de By. Spatiotemporal compression techniques for moving point objects. In *EDBT*, 2004.
21. R. Metha and V.K.Mehta. *The Principles of Physics*. S Chand, 1999.
22. J. Muckell, J.-H. Hwang, C. T. Lawson, and S. S. Ravi. Algorithms for compressing gps trajectory data: an empirical evaluation. In *ACM-GIS*, 2010.
23. J. Muckell, P. W. Olsen, J.-H. Hwang, C. T. Lawson, and S. S. Ravi. Compression of trajectory data: a comprehensive evaluation and new approach. *GeoInformatica*, 18(3):435–460, 2014.
24. A. Nibali and Z. He. Trajic: An effective compression system for trajectory data. *TKDE*, 27(11):3138–3151, 2015.
25. J. O’Rourke, C. B. Chien, T. Olson, and D. Naddor. A new linear algorithm for intersecting convex polygons. *Computer Graphics and Image Processing*, 19(4):384–391, 1982.
26. T. Pavlidis and S. L. Horowitz. Segmentation of plane curves. *IEEE Transactions on Computers*, 23(8):860–870, 1974.
27. D. Pfoser and C. S. Jensen. Capturing the uncertainty of moving-object representations. In *SSD*, 1999.
28. I. S. Popa, K. Zeitouni, VincentOria, and A. Kharat. Spatio-temporal compression of trajectories in road networks. *GeoInformatica*, 19(1):117–145, 2014.
29. M. Potamias, K. Patroumpas, and T. K. Sellis. Sampling trajectory streams with spatiotemporal criteria. In *SSDBM*, 2006.
30. U. Ramer. An iterative procedure for the polygonal approximation of plane curves. *Comput. Graphics Image Processing*, 1:244–256, 1972.
31. K. Reumann and A. Witkam. Optimizing curve segmentation in computer graphics. In *International Computing Symposium*, 1974.
32. K.-F. Richter, F. Schmid, and P. Laube. Semantic trajectory compression: Representing urban movement in a nutshell. *Journal of Spatial Information Science*, 4(1):3–30, 2012.
33. F. Schmid, K. Richter, and P. Laube. Semantic trajectory compression. In *SSTD*, pages 411–416, 2009.
34. Shamos, M. Ian, and H. Dan. Geometric intersection problems. In *Symposium on Foundations of Computer Science*, pages 208–215, 1976.
35. W. Shi and C. Cheung. Performance evaluation of line simplification algorithms for vector generalization. *Cartographic Journal*, 43(1):27–44, 2006.
36. J. Sklansky and V. Gonzalez. Fast polygonal approximation of digitized curves. *Pattern Recognition*, 12:327–331, 1980.
37. R. Song, W. Sun, B. Zheng, and Y. Zheng. Press: A novel framework of trajectory compression in road networks. *PVLDB*, 7(9):661–672, 2014.
38. G. T. Toussaint. On the complexity of approximating polygonal curves in the plane. In *International Symposium on Robotics and Automation (IASTED)*, 1985.
39. G. Trajcevski, H. Cao, P. Scheuermann, O. Wolfson, and D. Vaccaro. On-line data reduction and the quality of history in moving objects databases. In *MobiDE*, 2006.
40. C. M. Williams. An efficient algorithm for the piecewise linear approximation of planar curves. *Computer Graphics and Image Processing*, 8:286–293, 1978.
41. D. Zhang, M. Ding, D. Yang, Y. Liu, J. Fan, and H. T. Shen. Trajectory simplification: An experimental study and quality analysis. *PVLDB*, 9(11):934–946, 2018.
42. Z. Zhao and A. Saalfeld. Linear-time sleeve-fitting polyline simplification algorithms. In *Proceedings of Auto-Carto*, pages 214–223, 1997.
43. Y. Zheng, X. Xie, and W. Ma. GeoLife: A collaborative social networking service among user, location and trajectory. *IEEE Data Eng. Bull.*, 33(2):32–39, 2010.
44. A. Züfle, G. Trajcevski, D. Pfoser, M. Renz, M. T. Rice, T. Leslie, P. L. Delamater, and T. Emrich. Handling uncertainty in geo-spatial data. In *ICDE*, 2017.